

HAZMAT. V. The Ultraviolet and X-ray Evolution of K Stars

TYLER RICHEY-YOWELL,¹ EVGENYA L. SHKOLNIK,¹ ADAM C. SCHNEIDER,¹ ELLA OSBY,¹ TRAVIS BARMAN,² AND VICTORIA S. MEADOWS³

¹*School of Earth and Space Exploration, Arizona State University, Tempe, AZ 85281, USA*

²*Lunar and Planetary Laboratory, University of Arizona, Tucson, AZ 85721, USA*

³*NASA Astrobiology Institute, Virtual Planetary Laboratory, University of Washington, Seattle, WA 85215, USA*

(Accepted December 21, 2018)

Submitted to ApJ

ABSTRACT

Knowing the high-energy radiation environment of a star over a planet's formation and evolutionary period is critical in determining if that planet is potentially habitable and if any biosignatures could be detected, as UV radiation can severely change or destroy a planet's atmosphere. Current efforts for finding a potentially habitable planet are focused on M stars, yet K stars may offer more habitable conditions due to decreased stellar activity and more distant and wider habitable zones (HZ). While M star activity evolution has been observed photometrically and spectroscopically, there has been no dedicated investigation of K-star UV evolution. We present the first comprehensive study of the near-UV, far-UV, and X-ray evolution of K stars. We used members of young moving groups and clusters ranging in age from 10 – 625 Myr combined with field stars and their archived *GALEX* UV and *ROSAT* X-ray data to determine how the UV and X-ray radiation evolve. We find that the UV and X-ray flux incident on a HZ planet is 5 - 50 times lower than that of HZ planets around early-M stars and 50 - 1000 times lower than those around late-M stars, due to both an intrinsic decrease in K dwarf stellar activity occurring earlier than for M dwarfs and the more distant location of the K dwarf HZ.

Keywords: stars: evolution, stars: low-mass

1. INTRODUCTION

Astronomers have discovered thousands of exoplanets, with an estimate for the occurrence rate of Earth-sized planets in the habitable zone (HZ) around GK stars of 22% (Petigura et al. 2013) from the Kepler mission statistics. The *Transiting Exoplanet Survey Satellite* (*TESS*) is expected to detect yet another 3,500 planetary candidates during its mission life (Ricker et al. 2009, 2014; Barclay et al. 2018; Huang et al. 2018). While *TESS* is expected to discover \sim 700 new planets around K stars, none are expected to be in the HZ since *TESS* is optimized to find planets with short orbital periods, excluding the longer orbital periods of habitable zone planets around K stars (Barclay et al. 2018; Huang et al. 2018). However, the *PLAnetary Transits*

and Oscillations of stars (PLATO) mission, which will be optimized to find habitable zone planets around K dwarfs, is expected to discover \sim 30 HZ K dwarf planets in the next decade (PLATO Definition Study Report, 2017).

Further research is being conducted on what stellar characteristics increase the chances of HZ planets being in fact habitable (e.g. Cockell et al. 2016; Kaltenegger 2017). This would require a balance of environmental factors such as stellar lifetime, ultraviolet (UV) radiation, stellar winds, and HZ width. Currently, the most promising candidates for potentially habitable planets are thought to be around M stars (2,400 – 3,700 K; 0.08 – 0.45 M_⊕; conservative HZ width 0.1AU, Kopparapu et al. 2013); over half of all known HZ planets are around M dwarfs. Rocky planets around these stars are more easily detectable than around Sun-like stars due to favorable star-planet radius ratios, mass ratios, and shorter periods (Charbonneau & Deming 2007). However, these

Table 1. Mass estimates based on the spectral type to effective temperature transformations of [Pecaut & Mamajek \(2013\)](#) and the evolutionary models of [Baraffe et al. \(2015\)](#).

SpT	TW Hya	β Pic	Tuc-Hor	AB Dor	UMa	Hyades	Field
	10 Myr	24 Myr	45 Myr	149 Myr	300 Myr	625 Myr	5 Gyr
K0	1.30	0.98	0.90	0.93	0.92	0.92	0.89
K1	1.26	0.96	0.88	0.89	0.89	0.89	0.86
K2	1.20	0.93	0.86	0.86	0.86	0.86	0.83
K3	1.10	0.89	0.83	0.80	0.80	0.80	0.79
K4	0.98	0.83	0.80	0.75	0.75	0.75	0.74
K5	0.90	0.78	0.77	0.71	0.71	0.71	0.70
K6	0.78	0.74	0.72	0.63	0.65	0.66	0.65
K7	0.75	0.72	0.69	0.59	0.62	0.62	0.61
K8	0.72	0.71	0.66	0.57	0.60	0.60	0.60
K9	0.68	0.68	0.63	0.54	0.57	0.57	0.57
M0	0.59	0.62	0.60	0.51	0.56	0.53	0.53
M1	0.49	0.52	0.52	0.45	0.50	0.47	0.47

stars are typically the most active of all spectral types and HZ planets around them are close-in and most likely tidally locked (e.g. [Checlair et al. 2017](#); [Barnes & Rory 2017](#)). Planets around M stars that were initially expected to be likely habitable, such as Proxima Centauri b, are losing favorability due to excessive flaring ([MacGregor et al. 2018](#)). M stars have been shown to have the largest levels of stellar activity during their pre-main sequence, which lasts through the duration of the formation of the planet and both its primordial and secondary atmospheres ([Schneider & Shkolnik 2018](#); [Shkolnik & Barman 2014](#)). Additionally, the large magnetic fields (\sim kG) of most M stars has been shown to potentially create magma oceans or partial melt the mantle of close-in planets, leading to increased volcanism and strong outgassing of greenhouse gases ([Kislyakova et al. 2017, 2018](#)). K stars ($3,700 - 5,200\text{K}$; $0.6 - 0.9M_{\odot}$), with conservative HZ width of 0.4AU, ([Kopparapu et al. 2013](#)) may offer super-habitable conditions due to decreased stellar activity, lower magnetic field strengths, faster contraction onto the main sequence, and more distant and wider HZs. The highest potential of finding a truly habitable planet may lie with K stars.

The evolution of stellar activity as determined in the near-UV (NUV), far-UV (FUV), and X-ray wavelength regions has been studied in great detail for both GK stars (e.g. [Findeisen et al. 2011](#)) and M stars (e.g. [Stelzer et al. 2013](#); [Shkolnik & Barman 2014](#); [Schneider & Shkolnik 2018](#)) using archived *Galaxy Evolution Explorer* (*GALEX*; [Martin et al. 2004](#)) and *RÖntgenSATellit* (*ROSAT*; [Truemper 1982](#)) photometric data. However,

a comprehensive investigation of the high-energy radiation environments of K-type stars has yet to be performed. The purpose of this study is to fill in this gap in our understanding of stellar evolution.

1.1. The Importance of UV Data

The UV radiation incident on a planet is a critical factor in determining if that planet is potentially habitable and if any biosignatures could be detectable. UV radiation ionizes and photodissociates some of the most important molecules for the development of life (e.g. H_2O , H_2 , O_2 , CO_2 , H_2S , and OCS) and signatures that would be indicative of life (e.g. CH_4 , NH_3 , and N_2O) with potential for complete erosion of the atmosphere (e.g. [Kasting et al. 1993](#); [Lichtenegger et al. 2010](#); [Segura et al. 2010](#); [Hu et al. 2012](#)). UV radiation can be split into three regimes: the extreme-UV (EUV, $100\text{-}912\text{\AA}$), the far-UV (FUV, $912\text{-}1700\text{\AA}$), and the near-UV (NUV, $1700\text{-}3200\text{\AA}$) as defined in [Linsky & Güdel \(2015\)](#). The EUV heats and inflates a planets upper-atmosphere, exacerbating its erosion ([Koskinen et al. 2010](#); [Lammer et al. 2007](#)). Other than very limited data from the former *Extreme Ultraviolet Explorer* (*EUVE*) satellite, no information in this wavelength regime exists for stars other than the Sun. Any missions observing in the EUV will exclude most of the ionizing flux due to absorption by the ISM. These values are crucial as photochemical atmospheric models of HZ planets and abundance rate models require an input of EUV stellar fluxes, currently being interpolated from a limited number of FUV and X-ray observations.

Table 2. Number of K stars in each group or cluster.

Group/Cluster	Age	Input	Observed in NUV	Detected in NUV	Observed in FUV	Detected in FUV	Detected in X-ray
			[Myr]	Sample	by GALEX	by GALEX	by ROSAT
TWA	$10 \pm 3^{\text{a}}$	4	3	2	2	2	4
Beta Pic	$24 \pm 3^{\text{b}}$	30	21	19	16	15	27
Columba	42_{-4}^{+6}a	14	11	10	10	5	4
Carina	45_{-7}^{+11}a	3	1	1	1	1	3
Tuc-Hor	$45 \pm 4^{\text{a}}$	26	25	24	24	22	20
AB Dor	149_{-19}^{+51}a	12	11	6	10	10	12
Ursa Major	$414 \pm 23^{\text{c}}$	12	7	3	7	7	8
Praesepe	600 ^d	133	52	49	62	17	0
Hyades	$625 \pm 50^{\text{e}}$	169	110	97	92	30	52
Field	~ 5000	310	229	169	211	152	107

References— (a) Bell et al. (2015), (b) Shkolnik et al. (2017), (c) Jones et al. (2015, 2017), (d) Kraus & Hillenbrand (2007), (e) Perryman et al. (1997)

Realistic information regarding the evolution of the NUV, FUV, and EUV is of the utmost importance for using models to answer questions regarding planetary atmospheres. UV radiation, in particular the ratio of FUV/NUV, can impact the abundance rates and photochemistry of the atmospheres in the production of hazes in depleting atmospheres (Zerkle et al. 2012; Arney et al. 2017) and ozone in oxidizing atmospheres (Segura et al. 2003, 2005), both of which drastically alter the planetary spectrum. This affects not only the composition, but also the detectability and stability of the atmospheres of these planets. For future missions such as the *James Webb Space Telescope (JWST)* that will focus on spectra, a planet with a hazy or depleted atmosphere will not make a good target.

1.2. The K Star Advantage

While current popularity resides among M stars as the most likely to host identifiable habitable planets, stellar variability, excess flaring and tidal locking in the HZ is cause for concern (e.g. Shields et al. 2016). Early and mid-K spectral-type stars have been suggested by Heller & Armstrong (2014) to be “super-habitable”, i.e. the probability of life on a planet orbiting in the HZ of one of these super-habitable stars is higher than the probability of life on an Earth-sized planet orbiting in the HZ of a G2V star. Cuntz & Guinan (2016) analyzed several factors to determine the Habitable-Planetary-Real-Estate Parameter (HabPREP), which depends on the frequency of different stars, the rate of contraction onto the main sequence, the size and longevity of the HZ, UV and X-ray emission and flare frequency and power. They individually determined that the highest probability of having a habitable planet is in the early-K star regime.

The longer lifetimes of the continuous HZ of these types of stars compared to F and G stars allow for life to tune their environment and develop a more favorable biosignature, whereas unmagnetized planets around M stars may lose their atmosphere within the first 100 Myr based on severe UV irradiance (Airapetian et al. 2017). Lingam & Loeb (2017) find that K6V stars around $0.67 M_{\odot}$ would take the least amount of time for complex life to develop since increased oxygen levels from UV photolysis permit the emergence of complex life. Arney et al. (2018) have independently concluded that there is a similar K star advantage because a planet orbiting a K6V star has the potential to produce detectable CH₄ and O₂. However, the UV flux for most of these calculations was assumed to be constant throughout the timescale of the formation of life and could consequently lead to incorrect determinants. K star UV evolution is thus needed to determine the probability of planetary habitability. The highest potential of finding a truly habitable planet may lie with K stars.

2. THE K STAR SAMPLE

We compiled K stars in young moving groups (YMG) and clusters ranging in age from 10 Myr to 625 Myr. The associations included are TW Hydra (10 ± 3 Myr, Bell et al. 2015), Beta Pictoris (24 ± 3 Myr, Shkolnik et al. 2017), Columba (42_{-4}^{+6} Myr, Bell et al. 2015), Carina (45_{-7}^{+11} Myr, Bell et al. 2015), Tucana-Horologium (45 ± 4 Myr, Bell et al. 2015), AB Doradus (149_{-19}^{+51} Myr, Bell et al. 2015), Ursa Majoris (414 ± 23 Myr; Jones et al. 2015, 2017), Praesepe (600 Myr, Kraus & Hillenbrand 2007), and Hyades (625 ± 50 Myr, Perryman et al. 1997). In addition, we define a field star sample as K stars within 30 pc to which we assign an

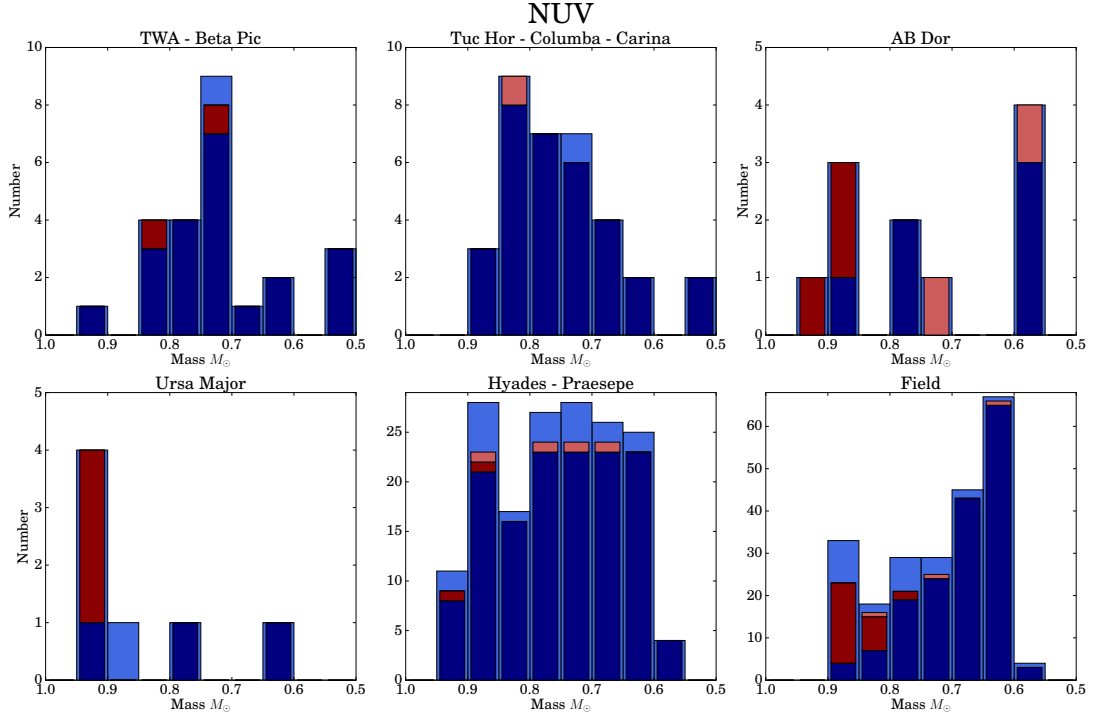


Figure 1. Stacked histograms showing the mass distributions for the input and returned targets in the GALEX NUV for each age group. Light blue represents the input sample, dark blue are the detections with no photometric flags, dark red are the lower limits, and light red are the upper limits.

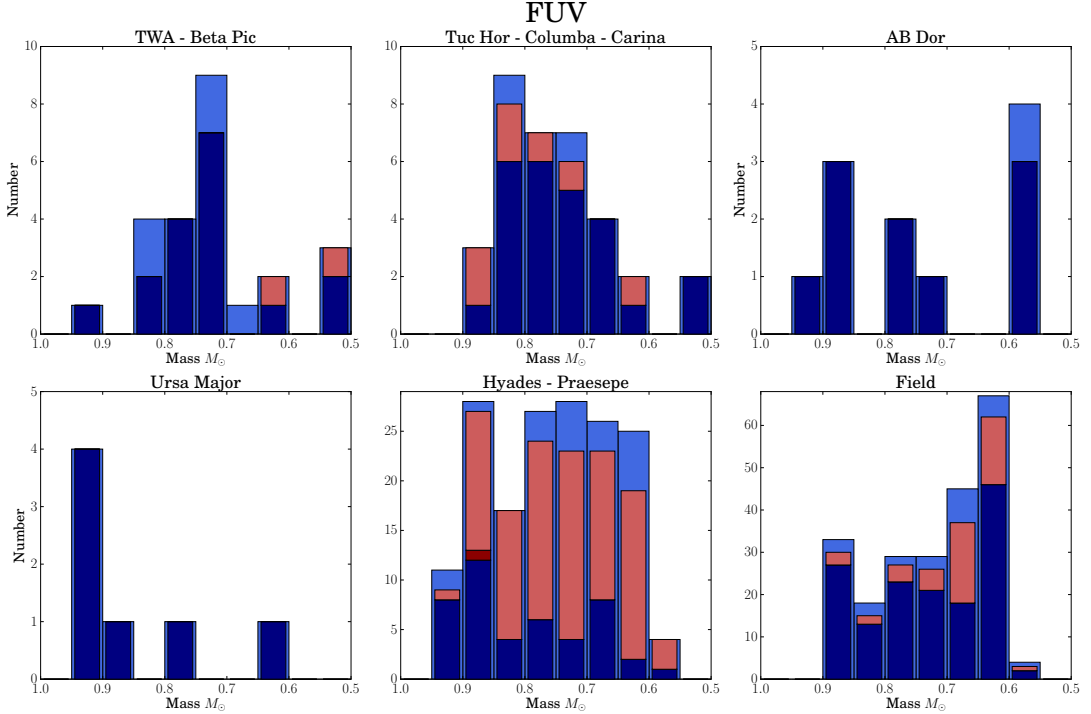


Figure 2. Same as Figure 1 but for GALEX FUV targets.

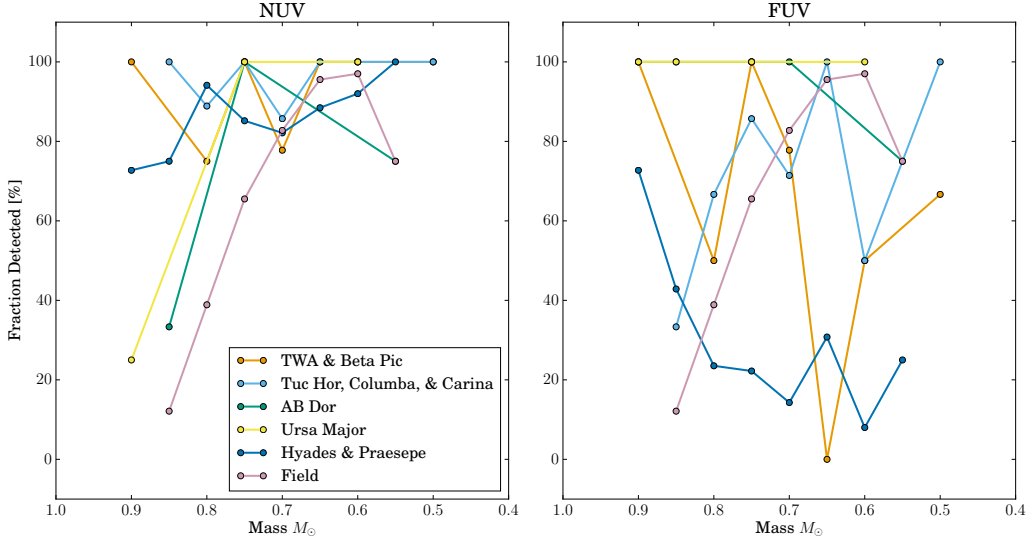


Figure 3. Percentages of targets detected by *GALEX* without any artifacts or flags compared to the input sample as a function of stellar mass. Groups of similar ages were combined to avoid issues due to small number statistics. In the NUV, higher-mass stars with a magnitude < 15 , i.e. in the non-linear regime, were considered instead as lower limits. The low return of Hyades and Praesepe members in the FUV is due to the clusters’ further distances of 47pc and 177pc, respectively (van Leeuwen 2009).

age of 5 Gyr. The sample was drawn from SIMBAD and confirmed individually to not be close binaries or known association members.

Taking into account the wide range of ages in this study, we must consider how similar spectral types represent different masses over various ages. Using the effective stellar temperatures in Pecaut & Mamajek (2013) and the model isochrones from Baraffe et al. (2015), we determine mass estimates for the spectral types used in this work following Table 1. We used masses from $0.6 - 0.9 M_{\odot}$ but allowed one spectral subtype lower and higher to account for spectral type uncertainty.

The YMG members were identified by Gagné et al. (2017) for TW Hydra; Shkolnik et al. (2017) for Beta Pictoris; Malo et al. (2013) for Carina, Columba, and AB Doradus; Kraus et al. (2014) for Tucana Horologium; Montes et al. (2001) for Ursa Major; Wang et al. (1995) for Praesepe; and Goldman et al. (2013) for the Hyades. Due to the low number of K star members in some of the age ranges, we combined groups of similar age ranges to calculate the median and inner quartiles for each age bin, as seen in Figures 1 and 2.

3. GALEX PHOTOMETRY

We cross referenced proper motion corrected coordinates of our sample to *GALEX* using the *GALEXview*

tool¹ with a search radius of $10''$. The NUV ($1771 - 2831 \text{ \AA}$) and FUV ($1344 - 1786 \text{ \AA}$) detectors have a non-linear response at $104 \text{ counts s}^{-1}$ and 34 counts s^{-1} , respectively, equivalent to a magnitude of ≈ 15 for both NUV and FUV. Measured magnitudes less than 15 were thus taken as lower limits. Additionally, we excluded detections with photometric flags for bright star window reflection, dichroic reflection, detector run proximity, or bright star ghost. We visually inspected the *GALEX* tiles for each observation to ensure that there was no contamination that was not caught by the flags. A comparison of the number of objects that were in our input sample, observed by *GALEX*, and were then resolved with no photometric flags for each band can be seen in Table 2 and Figure 3.

In the NUV, the higher mass objects were less likely to have usable photometry, as they were too bright for reliable photometric measurements. This is due to the more massive stars being intrinsically brighter and saturating the detector. For the Hyades and Praesepe clusters, the low fraction of detections is most likely due to their distances (47 pc and 177 pc, respectively; van Leeuwen 2009).

For some objects there were multiple observations with multiple exposure times, in which case we took the weighted mean of the magnitude as our measurement and the weighted standard deviations as our un-

¹ <http://galex.stsci.edu/galexview/>

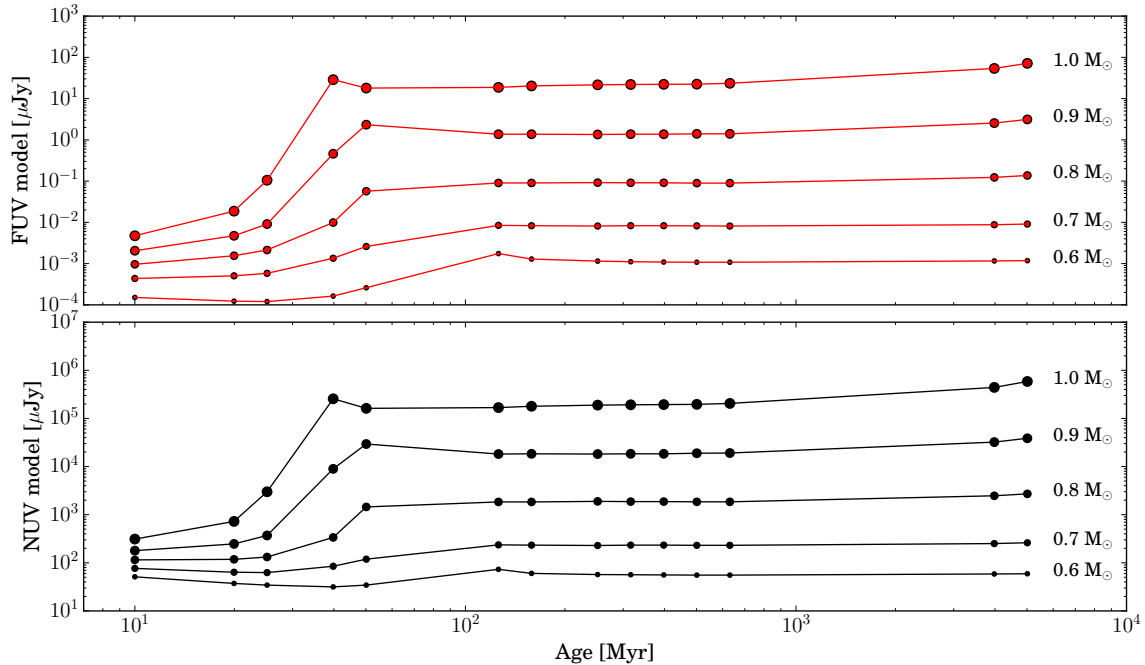


Figure 4. Photospheric FUV and NUV flux densities calculated from the PHOENIX stellar atmosphere models as a function of age. Increasing point size represents increasing mass of the star from $0.6 - 1.0 M_{\odot}$. The $1.0 M_{\odot}$ model is included for reference to the Sun.

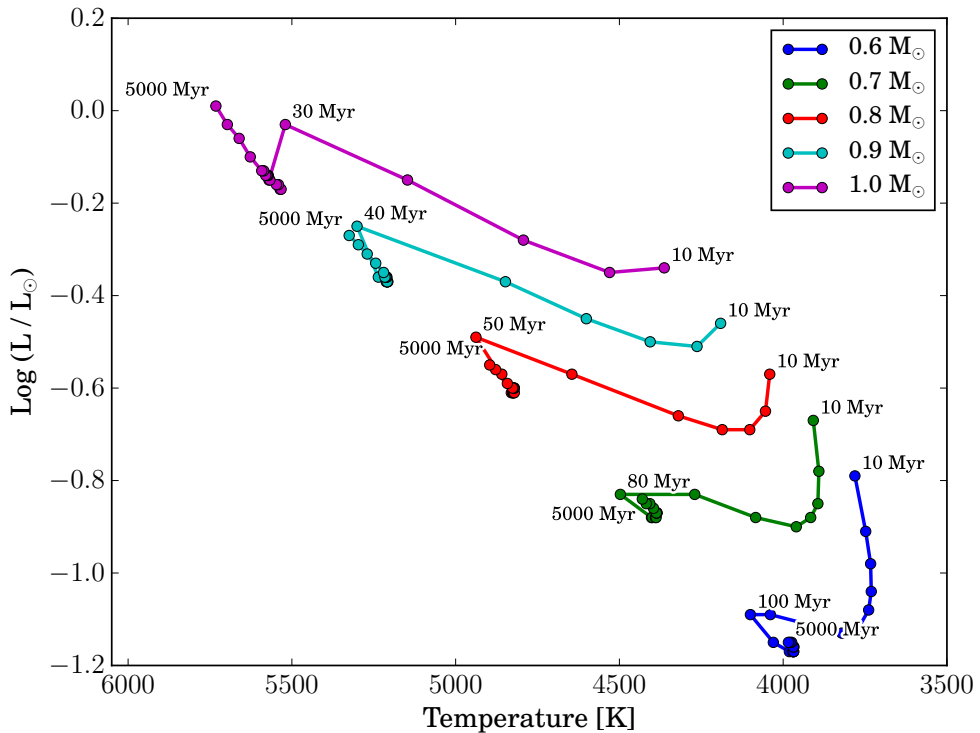


Figure 5. H-R diagram showing the evolutionary tracks of stars from $0.6 - 1.0 M_{\odot}$ using the results of Baraffe et al. (2015). Representative ages have been labeled to help guide the reader. Comparing this with Figure 4, it is clear that the drastic temperature change of pre-main sequence stars leads to a significant increase in the photospheric flux density, whereas the temperature (and thus the photospheric flux density) of main sequence stars is fairly constant.

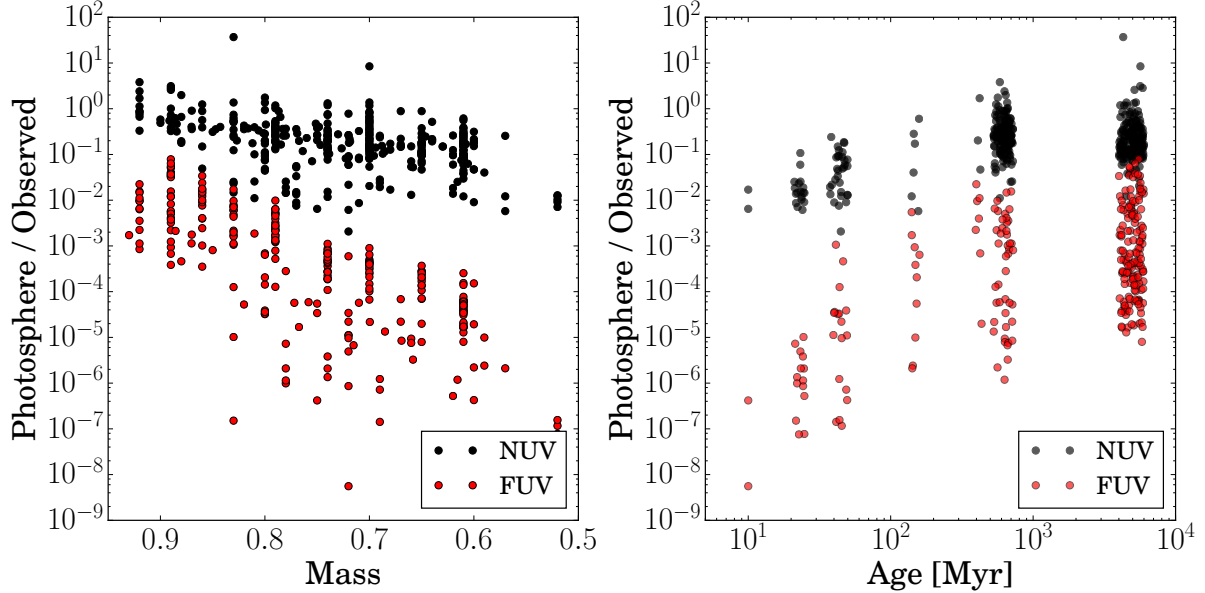


Figure 6. Fraction of the photospheric NUV and FUV flux densities compared to the observed as a function of mass (left) and age (right). Fractions above 1 are caused by uncertainties in the stellar mass, age, or model and were taken to be equal to 1 in our analysis. Ages have been moved from abscissa for clarity.

certainty. All of the photometry can be seen in Table 4.

For the objects that were observed but not detected, we calculated an upper limit for the object by repeating the search with a 10' radius and proceeding using the method described in Schneider & Shkolnik (2018). The objects that were measured with a magnitude <15 were taken as upper limits. These were then addressed in the same manner as the detections.

4. EVOLUTION OF THE PHOTOSPHERIC UV EMISSION

One of the goals of the HAZMAT program is to provide measurements of FUV and NUV flux densities for low-mass stellar models. Most low-mass stellar atmosphere models predict photospheric emission only and do not contain contributions from the stellar upper-atmosphere, leading to an underestimate of stellar photospheric emission. Work is being carried out to include contributions from these regions (i.e. Peacock et al. 2015, Fontenla et al. 2016), but observations are needed to fully inform these models with empirical data in the NUV and FUV.

The PHOENIX stellar atmosphere models (Hauschildt et al. 1997, Short & Hauschildt 2005) were used to calculate the photospheric NUV and FUV flux densities of each K star in our sample using the stellar masses derived in Table 1 and the age of the star. The evolution of the NUV and FUV photospheric model flux densities for select masses from 0.6 to 0.9 M_⊙ with a

reference 1 M_⊙ can be seen in Figure 4. As the mass increases, the photospheric contribution becomes greater. For each mass, the photospheric contributions become nearly constant after the age at which contraction onto the main sequence has ended, since the temperature of the star does not significantly change after the pre-main sequence evolution during the ages used in this study (Figure 5).

Figure 6 shows the fraction of the photospheric flux density compared to the absolute observed values for the YMG members and field stars as a function of both mass and age. The NUV has a higher fraction of photosphere compared to observed flux, with most of the contribution being between 10 and 100%. Values reported that were larger than 100% are due to uncertainties in both the mass and age of the star and were taken to be 100% photospheric. The photospheric FUV flux density was typically <1%. For both the NUV and the FUV we see a decrease in photospheric flux with decreasing mass, although this trend is much steeper for the FUV, where the photospheric contribution becomes negligible. With increasing age, we see an increase in photospheric contribution equally for both NUV and FUV flux densities.

For each of the YMG members and field stars, we subtract the photospheric contribution derived from the PHOENIX models from the absolute observed *GALEX* flux densities to calculate the excess emission, representative of upper-atmosphere activity.

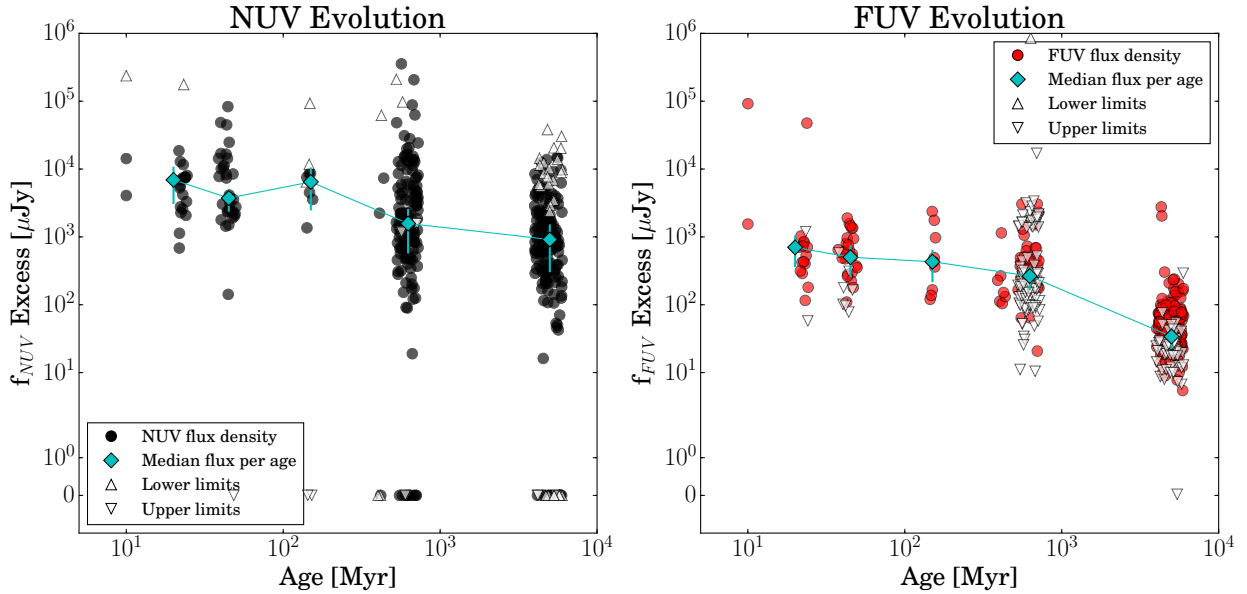


Figure 7. Absolute NUV (left) and FUV (right) excess flux density (i.e. photosphere-subtracted). The cyan diamonds represent the median value of the detections, upper limits, and lower limits for each age group. The error bars represent inner quartiles. Upper limits are shown by downward triangles and lower limits with upward triangles. Ages have been moved from abscissa for clarity. Typical errors are smaller than the markers.

5. EVOLUTION OF THE OBSERVED NUV AND FUV EMISSION

With the second data release of *Gaia* (Gaia Collaboration et al. 2018), accurate distances to all objects in our sample are available. Therefore, we investigate the absolute *GALEX* NUV and FUV flux densities rather than analyzing them relative to the Two Micron All-Sky Survey (2MASS) J-band, such as in Shkolnik & Barman (2014) and Schneider & Shkolnik (2018).

To explore the evolutionary trends, we convert the *GALEX* reported magnitudes to flux densities in μJy using

$$f_{\text{GALEX}} = 10^{\frac{23.9 - m_{\text{GALEX}}}{2.5}} \quad (1)$$

where m_{GALEX} is the *GALEX* FUV or NUV magnitude. These values were then translated to absolute fluxes using the known distances from *Gaia* Data Release 2 (Gaia Collaboration et al. 2018). Because we are interested in the excess UV contribution from the K stars, we calculated the photospheric contribution using the PHOENIX models as described in section 4 and subtracted these from the flux density calculations reported in *GALEX*.

Figure 7 shows the evolution of the excess NUV and FUV flux densities as a function of age. Both the NUV and FUV decrease in time. The slope of the decrease is much more gradual for the NUV than that of the FUV and the values obtained for early M stars in Shkolnik

& Barman (2014) and mid- to late M stars in Schneider & Shkolnik (2018). Unlike both Shkolnik & Barman (2014) and Schneider & Shkolnik (2018) where the median values remain constant up until 625 Myr and then distinctly drop off, we see a more gradual decrease in time starting at 100 Myr in the FUV. The wide spread comes from intrinsic astrophysical variation and perhaps initial spin rate, which has been shown to cause large spreads in the X-ray due to the bimodal distribution of stellar rotation in young open clusters for solar-like stars (Gondoin 2017, 2018). Additionally, the uncertainty in stellar ages beyond the age of the Hyades may cause increased variation among the field stars.

Figures 8 and 9 show the distribution of the NUV and FUV excess flux for the different age groups. The scatter in the FUV ranges from 1.5 – 3 orders of magnitude, similar to Shkolnik & Barman (2014). Shkolnik & Barman (2014) and Schneider & Shkolnik (2018) see a change in the median FUV value of about 1.5 orders of magnitude for stars with masses $0.35 - 0.6 M_{\odot}$, whereas for the K stars we see a shift of only 1 order of magnitude. For the NUV, the scatter ranges from 1 – 4 orders of magnitude, with the scatter increasing for the older age groups. The slopes of the NUV and FUV excess flux density vs age curves are found in Table 3. These trends can be used to predict flux densities and their ranges for K stars in the NUV and FUV bands.

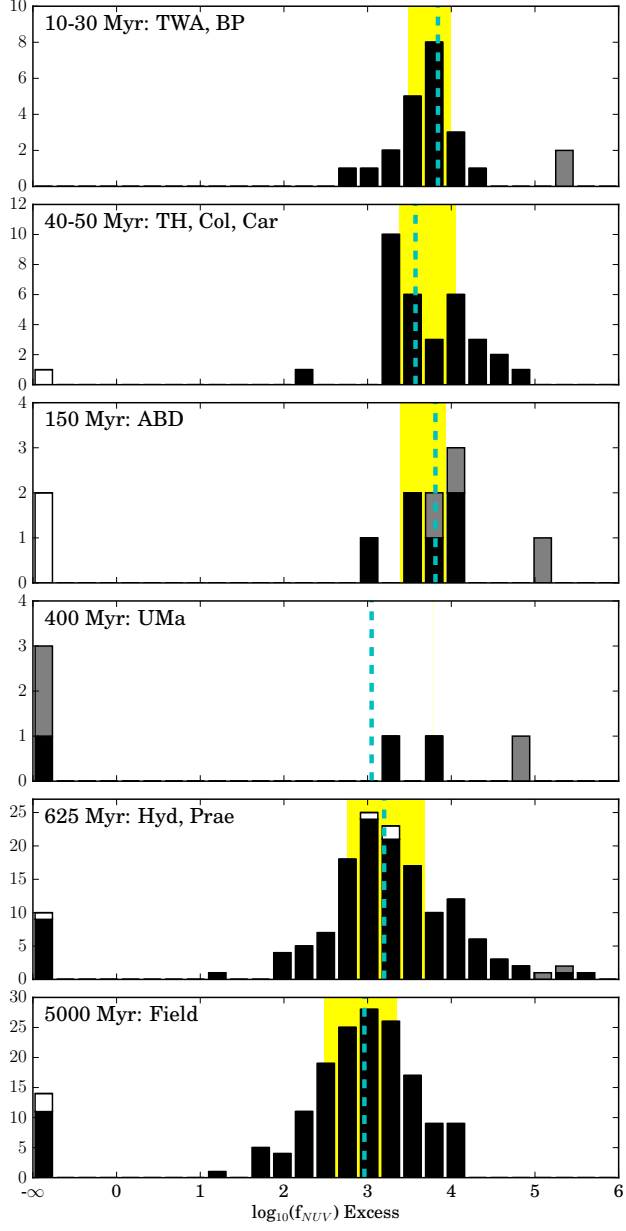


Figure 8. Histogram of NUV excess flux densities. Median values are shown by cyan dashed lines. The yellow areas represent the inner quartiles. Upper limits are shown in white and lower limits in gray. The negative infinity values are stars with zero excess.

5.1. Mass Distributions

Figure 10 is the same as Figure 7 but broken down by mass group. In both the NUV and FUV, we see that in general, all three mass groups follow the trends of each other. This is counter to the trends seen in Schneider & Shkolnik (2018), where the late M stars remain active much longer than early M stars. Even though the

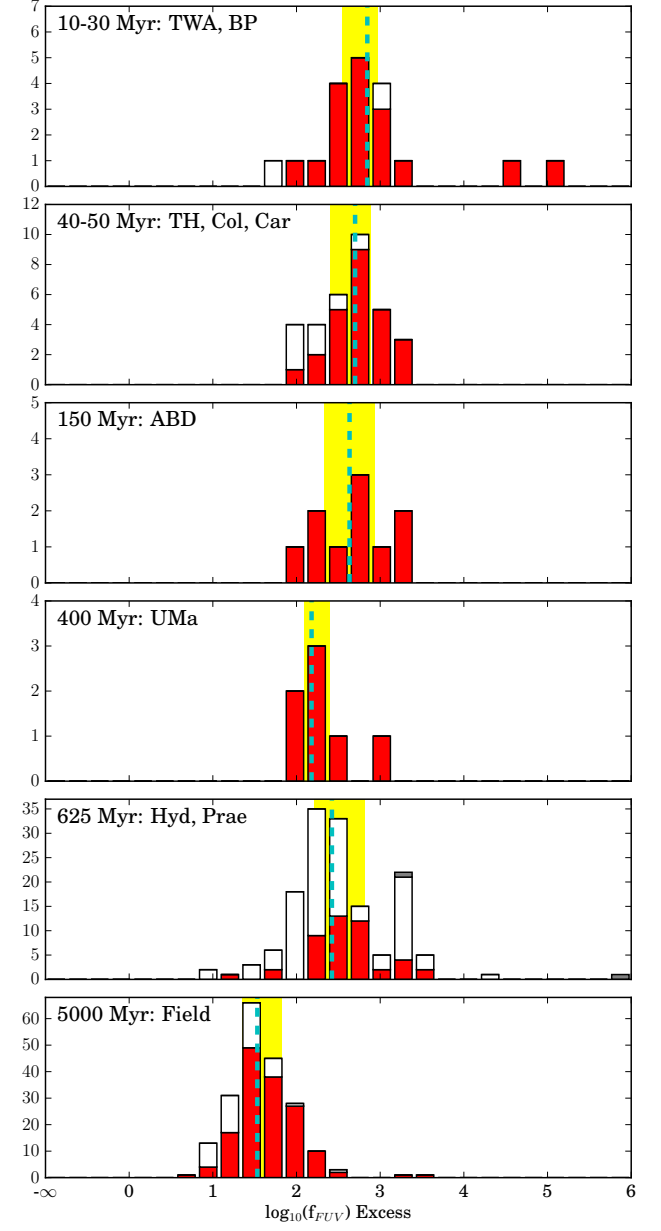


Figure 9. Same as Figure 8 but for FUV excess flux density. Median values are shown by cyan dashed lines. The yellow areas represent the inner quartiles. Upper limits are shown in white and lower limits in gray.

higher-mass stars have a larger contribution from the photosphere that is being subtracted off to yield the excess, the intrinsic flux of the higher-mass stars is large enough that the excess flux is still largest for higher-mass stars throughout most of the evolutionary period. However, once the stars reach field age, the photospheric contribution becomes so large that most of the excess flux for higher-mass stars approaches zero.

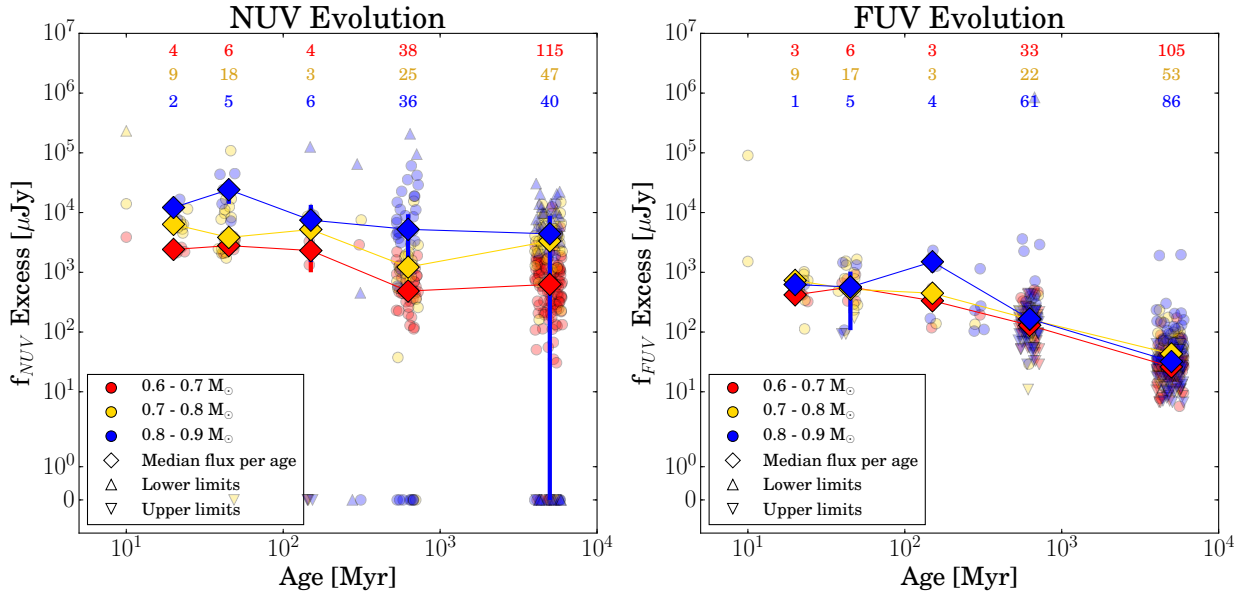


Figure 10. Absolute NUV (left) and FUV (right) excess flux density (i.e. photosphere-subtracted) separated by mass. The diamonds represent median values and the lines the inner quartiles. The large inner quartile for the early K stars at the field age is due to a large number of stars without excess flux. The number of stars in each age and mass bin are shown at the top. Typical errors are smaller than the markers.

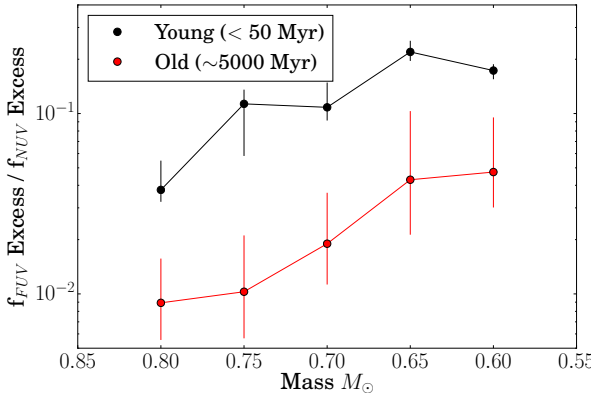


Figure 11. Ratio of FUV Excess to NUV Excess as a function of mass. The ratio is clearly mass and age dependent.

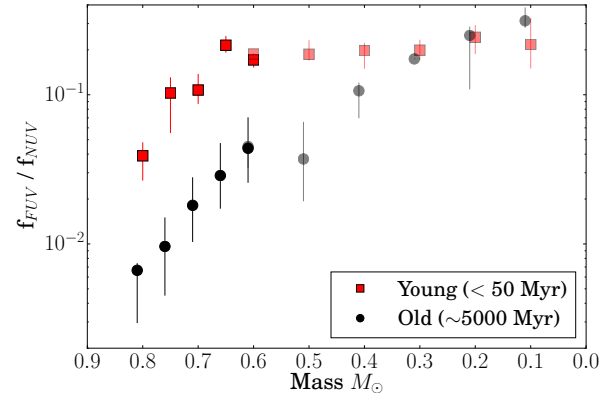


Figure 12. Ratio of FUV to NUV as a function of mass for K stars (opaque) from this work and M stars (translucent) from Schneider & Shkolnik (2018). In this case the photosphere has not been subtracted for either K or M stars.

6. THE RELATIONSHIP BETWEEN GALEX FUV AND NUV FOR K STARS

6.1. FUV / NUV

The ratio of FUV to NUV is valuable in understanding the photochemistry of terrestrial planet atmospheres. Segura et al. (2005) showed that lifetimes of the biogenic gases CH₄, N₂O, and CH₃Cl are actually increased, allowing a higher probability of being detected. However, the FUV to NUV ratio also sets the abundance rates of molecules such as CO₂, O₂, and O₃, as the FUV will break down CO₂, forming O₂ and O₃, the latter of which

will be destroyed by the NUV. This abiotic oxygen and ozone can thus produce false-positive biosignatures (e.g. Domagal-Goldman et al. 2014; Tian et al. 2014; Harman et al. 2015).

We calculate FUV/NUV excess flux densities as a function of mass for stars with both NUV and FUV flux densities, as seen in Figure 11. The trends seen in Schneider & Shkolnik (2018) continue into the K-star regime, with increasing separation between the young and old stars as the stellar mass increases, demon-

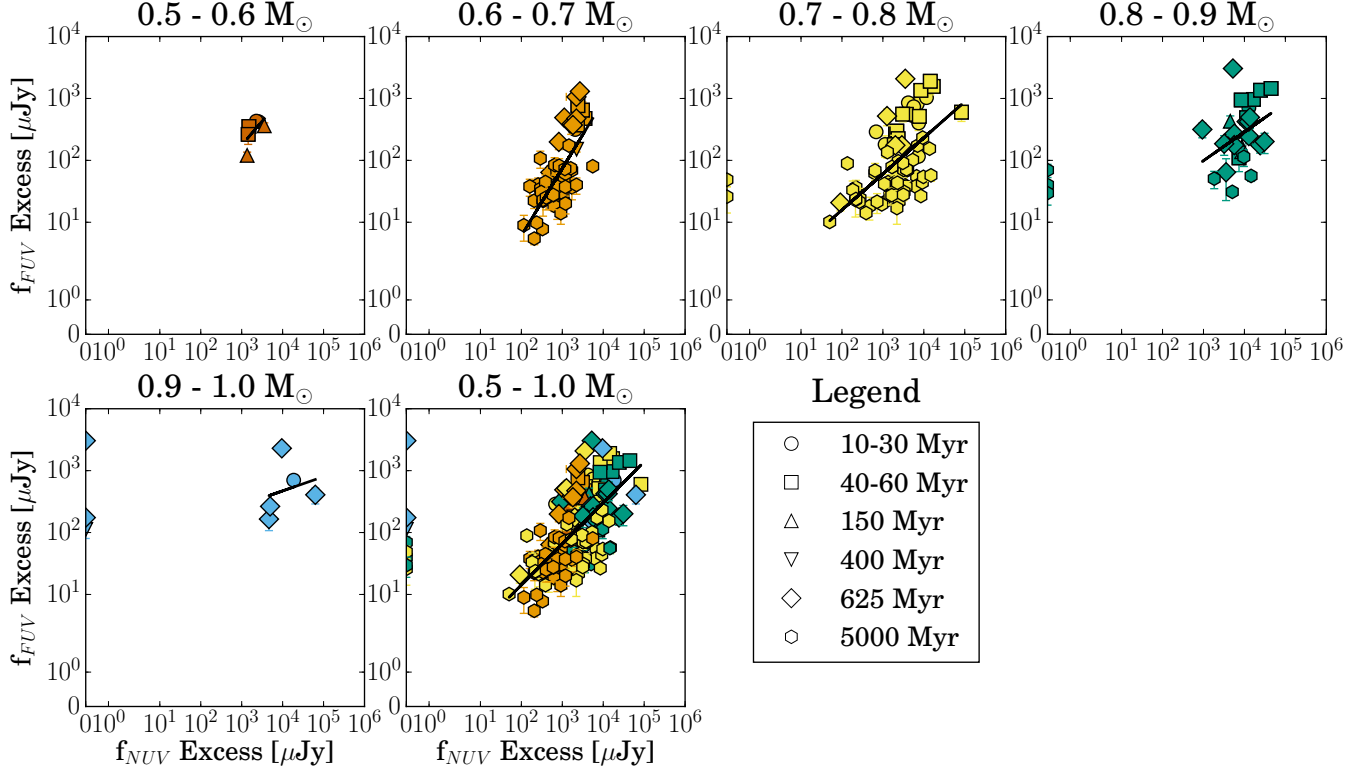


Figure 13. FUV excess flux density versus NUV excess flux density for different mass bins. The parameters for the best fit lines can be found in Table 3. The zero excess points were not included in the calculation of the trend lines. Typical errors are smaller than the markers.

ing that the FUV/NUV ratio is both mass- and age-dependent.

6.2. NUV vs FUV

When comparing the NUV to FUV excess flux density, we do not see the same tight correlations as Shkolnik & Barman (2014) nor Schneider & Shkolnik (2018). Instead, we see in Figure 13 that with increasing mass (i.e. earlier spectral type), the scatter becomes greater and the correlation worsens. We calculated both a Pearson's R^2 statistic (Pearson 1895) and a Spearman Rank correlation value (Spearman 1904) for each K spectral type mass range. The results can be seen in Figure 14. In both tests we see a similar trend, where the highest mass (i.e. earliest spectral type) stars have correlations generally with $\rho < 0.5$ and lower mass (i.e. later spectral type) stars have correlations generally $\rho > 0.5$. This trend also appears in Miles & Shkolnik (2017).

The reason for this decrease in correlation with higher mass can most easily be seen in analyzing the model photospheric fluxes in Figure 4. In comparing the model values of a single mass from 10 Myr – 5 Gyr, the photospheric flux density of a $0.6 M_\odot$ star changes by no more than a single order of magnitude. However, the photospheric flux density of a $0.9 M_\odot$ star is much more

prevalent and changes by as much as four orders of magnitude. The scatter in the FUV excess flux density vs NUV excess flux density then comes from differences in age, whereas the intrinsic scatter of a single age group is much smaller.

7. X-RAY EVOLUTION

The X-ray flux has frequently been used as a stellar activity diagnosis (e.g. Jackson et al. 2012; Booth et al. 2017). X-ray wavelengths may be used in conjunction with the NUV and FUV to interpolate into the EUV, which is most powerful in understanding the photodissociation of molecules in a planet's atmosphere. To compare X-ray and UV data, we cross-referenced our sample of K stars with the Second ROSAT All-Sky Survey Point Source Catalog (2RXS, 5–124 Å; Boller et al. 2016) with a search radius of $38''$, which was determined by Voges et al. (1999) to be the 3σ positional error. We then used the hardness ratio and the count rate to convert to flux F_X in $\text{erg s}^{-1} \text{cm}^{-2}$ using the empirical fit of Schmitt et al. (1995). The number of detections can be seen in the last column of Table 2.

As can be seen in Figure 15, the X-ray flux remains steady through the age of Tucana-Horologium (45 Myr) and decreases by the age of AB Doradus (150 Myr), sim-

Table 3. Fits to $\log(y) = m * \log(x) + b$ in logarithmic space.

$\log(x)$ [μJy or Myr]	$\log(y)$ [μJy]	Subset	Slope (m)	Intercept (b)	R^2	No. ^a
NUV Excess	FUV Excess	0.5 - 0.6 M_\odot	0.784 ± 0.177	-0.107 ± 0.594	0.399	6
NUV Excess	FUV Excess	0.6 - 0.7 M_\odot	1.086 ± 0.039	-1.387 ± 0.120	0.493	61
NUV Excess	FUV Excess	0.7 - 0.8 M_\odot	0.583 ± 0.025	0.033 ± 0.091	0.328	75
NUV Excess	FUV Excess	0.8 - 0.9 M_\odot	0.463 ± 0.074	0.605 ± 0.297	0.124	27
NUV Excess	FUV Excess	0.9 - 1 M_\odot	0.231 ± 0.123	1.750 ± 0.502	0.061	5
NUV Excess	FUV Excess	All	0.663 ± 0.016	-0.174 ± 0.056	0.418	174
X-ray	NUV Excess	All	0.360 ± 0.009	-6.888 ± 0.097	0.281	110
X-ray	FUV Excess	All	0.665 ± 0.012	-4.717 ± 0.130	0.745	130
Age	NUV Excess	10 Myr - 150 Myr	0.003 ± 0.472	-10.635 ± 0.836	0.000	3
Age	NUV Excess	150 Myr - 5 Gyr	-0.536 ± 0.343	-9.498 ± 0.976	0.877	3
Age	FUV Excess	10 Myr - 625 Myr	-0.266 ± 0.257	-11.280 ± 0.495	0.968	4
Age	FUV Excess	625 Myr - 5 Gyr	-0.987 ± 0.426	-9.275 ± 1.414	1.000	2
Age	X-ray	10 Myr - 150 Myr	-0.424 ± 0.467	-9.612 ± 0.746	0.981	3
Age	X-ray	150 Myr - 5 Gyr	-0.923 ± 0.285	-8.522 ± 0.881	0.999	3

^aNumber of data points used in each fit.

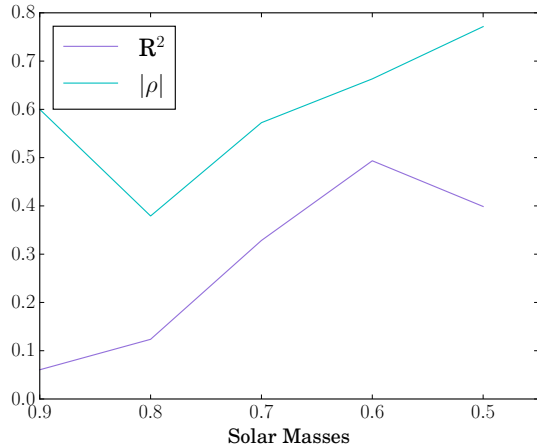


Figure 14. Pearson's R^2 correlation statistic and Spearman rank correlation for the trends seen in Figure 13. The correlations become worse at higher mass most likely due to the larger variation of photospheric contribution in age, as seen in Figure 4.

ilar to the trend in FUV. These results are also seen in Jackson et al. (2012), who see that FGKM stars remain saturated in the X-ray until about 100 Myr. We derive a slope of $(-0.906 \pm 0.079)\log(t)$ from 150 Myr - 5 Gyr (Table 3).

A histogram of the range in X-ray values for each age can be seen in Figure 16. The flux for each age ranges from 1-3 orders of magnitude, similar to the NUV and FUV values. Again, the wide spread likely comes from the bimodal distribution of stellar rotation in young

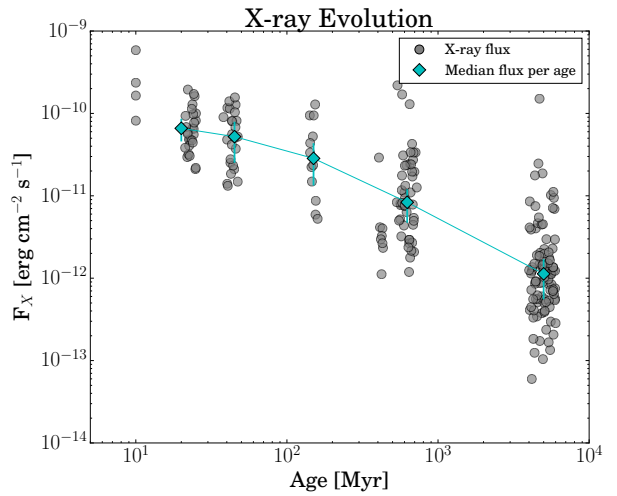


Figure 15. Same as Figure 7 but for X-ray flux (as compared to flux density).

open clusters for solar-like stars (Gondoin 2017, 2018) and uncertainty in stellar ages up to 10 Gyr among the field stars.

Unlike for the early-M stars in Shkolnik & Barman (2014), we do not see a clear distinction between young X-ray emitters and old emitters when looking at the UV flux compared to the X-ray flux (Figure 17). This may be due to larger spread in x-ray flux we see at the younger ages of K stars (Figure 16) and the more gradual decrease of the x-ray flux with age (Figure 18) as compared to the M stars in Shkolnik & Barman (2014),

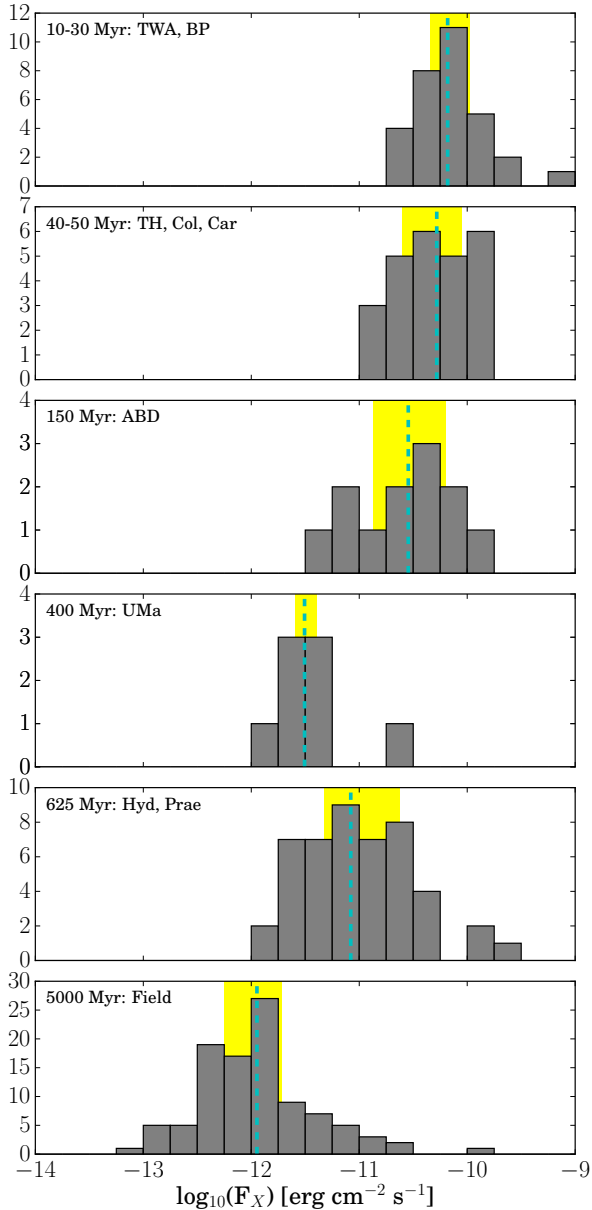


Figure 16. Same as Figures 8 and 9 but for X-ray flux. Median values are shown by cyan dashed lines. The yellow areas represent the inner quartiles.

leading to an undefined distinction between young and old emitters.

Figure 18 shows both the K and M star NUV, FUV, and X-ray fluxes (as opposed to flux densities) from this work, Shkolnik & Barman (2014), and Schneider & Shkolnik (2018). The M-star work was done relative to the J band flux, as the distances to the stars were not all known. We have therefore redone this work relative to the J band flux for comparison with the M stars. The results are extremely similar except for the K dwarf NUV median value at 150 Myr, which is noticeably ele-

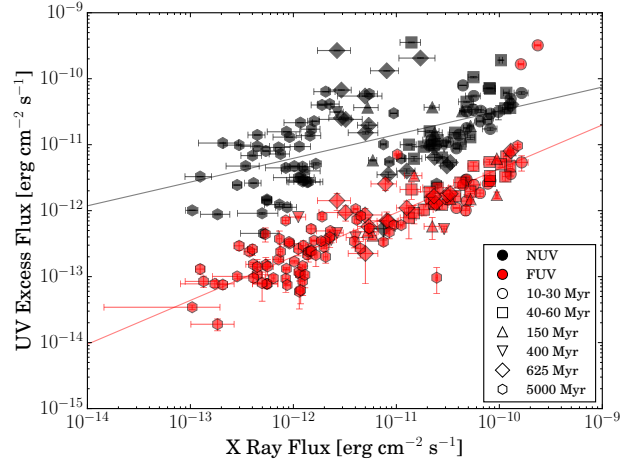


Figure 17. NUV and FUV Excess flux against X-ray flux from *ROSAT* for those stars with detections in both. Equations for the two fits are reported in Table 3.

vated. This is most likely due to small numbers in that age bin and uncertainties within the model photosphere, yet is still consistent within the inner quartiles seen in Figure 7

Comparing the K stars to the M stars, we see in both the FUV and the X-ray that at the age where a planet is forming its atmosphere (10 - 500 Myr; see Schaefer & Fegley 2010, and references therein), the K star flux has dropped below that of the M stars, meaning that any primordial atmosphere has a lower chance of being destroyed. In comparing the X-ray medians to those of the NUV and FUV, we see that the X-ray flux dominates during the young ages of the stars, then falls below the NUV values after 650 Myr, a trend also seen in the M dwarfs of Shkolnik & Barman (2014).

8. UV AND X-RAY FLUX AT THE HABITABLE ZONE

To better understand the habitability of planets around K stars, we need to understand what the UV and X-ray flux incident on a planet in the habitable zone would be. Using the radii and effective temperature estimates of Baraffe et al. (2015), we calculated the HZ distance as a function of age for a K star ($0.8 M_{\odot}$), an early-M star ($0.4 M_{\odot}$), and a late-M star ($0.1 M_{\odot}$) using Equation 3 of Kopparapu et al. (2013):

$$d = \left(\frac{R^2 \cdot T_{\text{eff}}^4}{S_{\text{eff}}} \right)^{0.5} \text{AU}, \quad (2)$$

where the stellar radius R and effective temperature T_{eff} are given in solar units and S_{eff} is the stellar photospheric flux at the HZ, which is strictly a function of the stellar temperature. The stellar flux at the HZ for each star was interpolated from the S_{eff} values given in

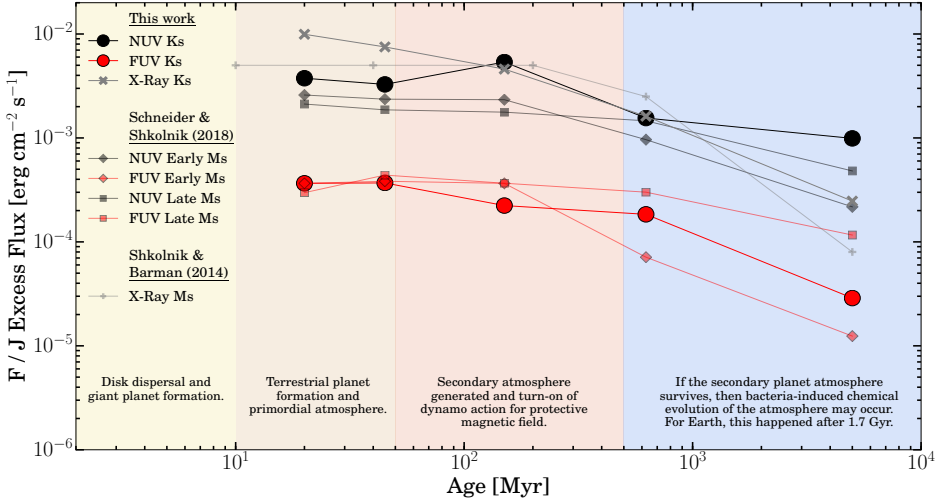


Figure 18. Median NUV and FUV fluxes as a function of age comparing the K stars in this work to the M stars in Schneider & Shkolnik (2018). The analysis of the K star NUV, FUV, and X-Ray evolution was redone similar to Shkolnik & Barman (2014) and Schneider & Shkolnik (2018), using the J band flux as a normalization for distance. The colored areas represent key evolutionary periods in a planet's formation.

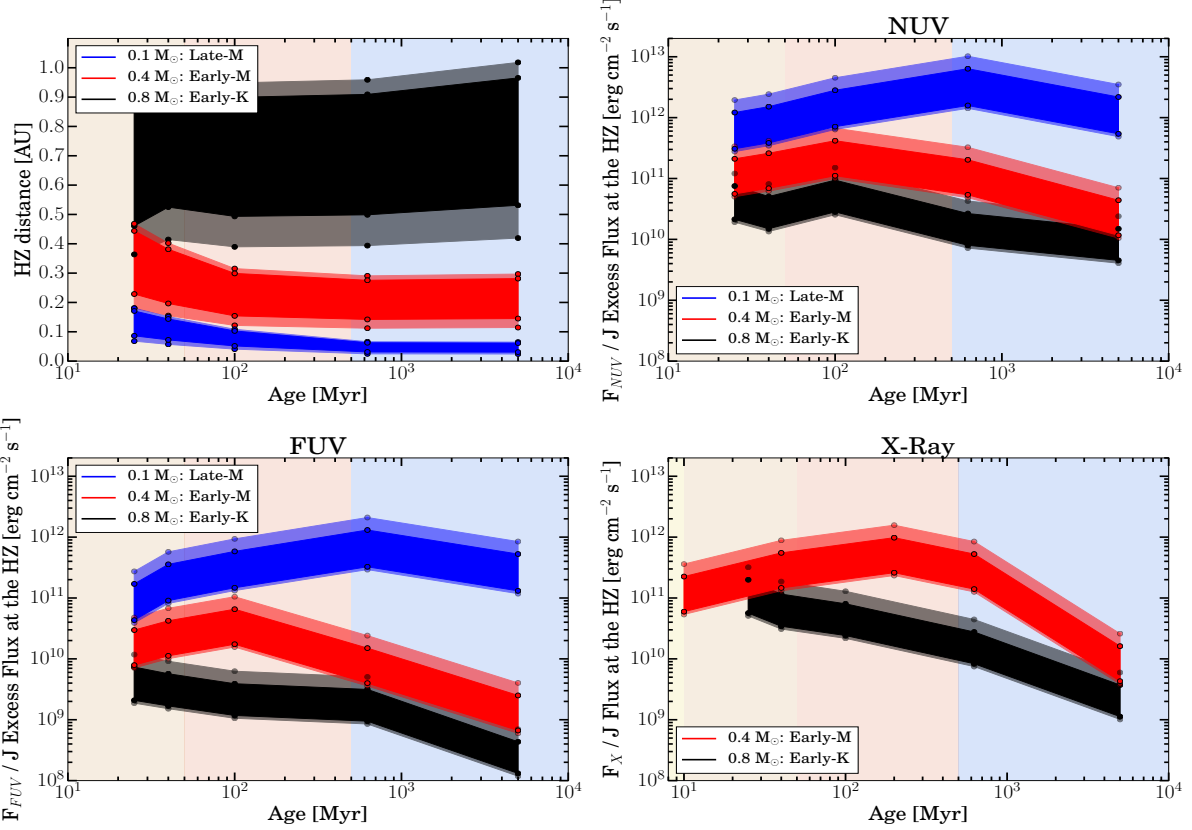


Figure 19. (a) Habitable zone distance from the star for a K star ($0.8 M_{\odot}$), an early-M star ($0.4 M_{\odot}$), and a late-M star ($0.1 M_{\odot}$). The opaque regions represent the conservative habitable zones and the translucent regions are the optimistic habitable zones. The color regions correspond to key planetary evolutionary periods outlined in Figure 18. (b, c, d) NUV, FUV, and X-Ray median excess flux in the conservative (opaque) and optimistic (translucent) habitable zone ranges, respectively.

Kopparapu et al. (2014) for temperatures from 2600 K - 7200 K. The HZ distances are shown in Figure 19a as a function of age. The opaque regions represent the conservative habitable zones and the translucent regions are the optimistic habitable zones. The size of the K-dwarf HZ is about twice as large as that of the M-stars and farther from the star by at least 0.4 AU.

We then calculated the range of NUV, FUV, and X-ray median values in the HZ at each age, as seen in Figures 19b, 19c, and 19d, respectively. In each of the plots, the K-star flux levels are below those of the M-stars by at least five times for the early-M stars and at least 50 times for the late-M stars. The initial rise in the NUV, FUV, and X-ray flux of all of the M stars is due to the HZ becoming closer-in to the star as the star ages, thus increasing the UV and X-ray flux in this region. For this reason, the UV and X-ray HZ flux of late-M stars is larger during the early stages of planet evolution than when the planet was initially formed. Conversely, the UV and X-ray HZ flux of K stars decreases from the time of planet formation, thus allowing more suitable conditions for the development and detectability of life, perhaps garnering K dwarfs the “superhabitable” label.

9. IMPLICATIONS AND CONCLUSIONS

Because of their high-energy radiation environments, more frequent flaring, and tidally locked planets, M stars may not be the most suitable locations for finding habitable planets. Instead, if high UV emission is detrimental, then K stars offer a more favorable UV environment throughout the key evolutionary period of the planet and its atmosphere due to wider habitable zones and faster contraction onto the main sequence.

Using *GALEX* and *ROSAT* photometry, we calculated the NUV and FUV excess (i.e. photosphere subtracted to yield the emission from the upper-atmosphere) flux densities and X-ray flux levels from young moving group members, clusters, and field stars ranging from 10 Myr to 5 Gyr. We find that the FUV and X-ray fluxes remain constant for \sim 100 Myr before decreasing, as compared to M stars, which remain constant until \sim 650 Myr (Shkolnik & Barman 2014; Schneider & Shkolnik 2018). To determine the extent of the potential “super-habitability” of K stars, we also analyzed these results within the habitable zones of K and M stars. We find that the UV and X-ray flux incident on a planet is 5 - 50 times lower than that of early-M stars and 50 - 1000 times lower than that of late-M stars (depending on age). These UV and X-ray levels offer a much more suitable environment and a higher probability of planet habitability and the detection of any biomarkers.

These results should be used to advise estimations of the extreme-UV, for which very little data currently exist. The EUV fluxes are some of the most effective measures of chemical alteration, as the photodissociation cross-sections are the largest for most molecules in this regime. The EUV flux is expected to follow the trends of both the FUV and X-ray emission. Therefore, we would expect the EUV to decline as early as \sim 100 Myr.

The ratio of FUV to NUV is an important determinate in the probability of detecting a habitable planet. Larger ratios allow for longer lifetimes of biogenic gases such as as CH₄, N₂O, and CH₃Cl, leading to a higher probability of detection. However, this ratio also affects the abundances of abiotic molecules such as CO₂, O₂, and O₃ that may lead to false positive signatures. We find that this ratio is both mass- and age-dependent for all K spectral types.

While these results are informative of median UV and X-ray fluxes incident on K star planets during the early stages of their evolution, this does not entail a higher probability of habitability in the case of all K dwarfs.

The authors would like to acknowledge support from the NASA Habitable Worlds grant NNX16AB62G. We wish to thank the anonymous referee for an insightful and helpful report. This work is based on observations made with the NASA *Galaxy Evolution Explorer* and the *RÖntgenSATellit*. *GALEX* is operated for NASA by the California Institute of Technology under NASA contract NAS5-98034. This research utilized the public data from the second ROSAT All-Sky Survey (<https://heasarc.gsfc.nasa.gov/W3Browse/rosat/rass2rxs.html>). This work makes use of data products from the Two Micron All-Sky Survey, which is a joint project of the University of Massachusetts and the Infrared Processing and Analysis Center/California Institute of Technology, funded by the National Aeronautics and Space Administration and the National Science Foundation. This research has made use of the SIMBAD database, operated at CDS, Strasbourg, France. This work has made use of data from the European Space Agency (ESA) mission *Gaia* (<https://www.cosmos.esa.int/gaia>), processed by the Gaia Data Processing and Analysis Consortium (DPAC, <https://www.cosmos.esa.int/web/gaia/dpac/consortium>).

Software: Astropy (Price-Whelan et al. 2018), Matplotlib (Hunter 2007), Numpy (van der Walt et al. 2011), Scipy (Jones et al. 2001), PHOENIX (Hauschildt et al. 1997; Short & Hauschildt 2005)

REFERENCES

- Airapetian, V. S., Glocer, A., Khazanov, G. V., et al. 2017, *ApJ*, 836, L3
- Arney, G., Domagal-Goldman, S. D., & Meadows, V. 2018, in American Astronomical Society Meeting Abstracts, Vol. 231, American Astronomical Society Meeting Abstracts #231, 427.08
- Arney, G. N., Meadows, V. S., Domagal-Goldman, S. D., et al. 2017, *ApJ*, 836, 1, 49, 19 pp. (2017)., 836, arXiv:1702.02994
- Baraffe, I., Homeier, D., Allard, F., & Chabrier, G. 2015, *A&A*, 577, A42
- Barclay, T., Pepper, J., & Quintana, E. V. 2018, *ApJS*, 239, 2
- Barnes, R., & Rory. 2017, *Celestial Mechanics and Dynamical Astronomy*, 129, 4, pp.509-536, 129, 509
- Bell, C. P. M., Mamajek, E. E., & Naylor, T. 2015, *MNRAS*, 454, 1, p.593-614, 454, 593
- Boller, T., Freyberg, M. J., Trümper, J., et al. 2016, *A&A*, 588, A103
- Booth, R. S., Poppenhaeger, K., Watson, C. A., Silva Aguirre, V., & Wolk, S. J. 2017, *MNRAS*, 471, 1012
- Charbonneau, D., & Deming, D. 2007, eprint arXiv:0706.1047, arXiv:0706.1047
- Checlair, J., Menou, K., & Abbot, D. S. 2017, *ApJ*, 845, 2, 132, 10 pp. (2017)., 845, arXiv:1705.08904
- Cockell, C., Bush, T., Bryce, C., et al. 2016, *Astrobiology*, 16, 89
- Cuntz, M., & Guinan, E. F. 2016, *ApJ*, 827, 1, 79, 9 pp. (2016)., 827, arXiv:1606.09580
- Domagal-Goldman, S. D., Segura, A., Claire, M. W., Robinson, T. D., & Meadows, V. S. 2014, *ApJ*, 792, 90
- Findeisen, K., Hillenbrand, L., & Soderblom, D. 2011, *AJ*, 142, 1, 23, 17 pp. (2011)., 142, arXiv:1105.1377
- Fontenla, J. M., Linsky, J. L., Witbrod, J., et al. 2016, *ApJ*, 830, 154
- Gagné, J., Faherty, J. K., Mamajek, E. E., et al. 2017, *ApJS*, 228, 18
- Gaia Collaboration, Brown, A. G. A., Vallenari, A., et al. 2018, *A&A*, 616, A1
- Goldman, B., Röser, S., Schilbach, E., et al. 2013, *A&A*, 559, A43
- Gondoin, P. 2017, *A&A*, 599, A122
- . 2018, ArXiv e-prints, arXiv:1808.01824
- Harman, C. E., Schwertner, E. W., Schottelkotte, J. C., & Kasting, J. F. 2015, *ApJ*, 812, 137
- Hauschildt, P. H., Baron, E., & Allard, F. 1997, *ApJ*, 483, 390
- Heller, R., & Armstrong, J. 2014, *Astrobiology*, Vol. 14, No. 1, p. 50-66., 14, 50
- Hu, R., Seager, S., & Bains, W. 2012, *ApJ*, 761, 2, 166, 29 pp. (2012)., 761, arXiv:1210.6885
- Huang, C. X., Shporer, A., Dragomir, D., et al. 2018, arXiv e-prints, arXiv:1807.11129
- Hunter, J. D. 2007, *Computing in Science and Engineering*, 9, 90
- Jackson, A. P., Davis, T. A., & Wheatley, P. J. 2012, *MNRAS*, 422, 2024
- Jones, E., Oliphant, T., Peterson, P., et al. 2001, SciPy: Open source scientific tools for Python, [Online; accessed *today*.]
- Jones, J., White, R. J., Boyajian, T. S., et al. 2017, in American Astronomical Society Meeting Abstracts, Vol. 229, American Astronomical Society Meeting Abstracts #229, 131.05
- Jones, J., White, R. J., Boyajian, T., et al. 2015, *ApJ*, 813, 58
- Kaltenegger, L. 2017, *Annual Review of A&A*, 55, 433
- Kasting, J. F., Whitmire, D. P., & Reynolds, R. T. 1993, *Icarus*, 101, 108
- Kislyakova, K. G., Fossati, L., Johnstone, C. P., et al. 2018, *ApJ*, 858, 105
- Kislyakova, K. G., Noack, L., Johnstone, C. P., et al. 2017, *Nature Astronomy*, 1, 878
- Kopparapu, R., Ramirez, R., Kasting, J. F., et al. 2013, *ApJ*, 765, 2, 131, 16 pp. (2013)., 765, arXiv:1301.6674
- Kopparapu, R. K., Ramirez, R. M., Schottelkotte, J., et al. 2014, *ApJL*, 787, L29
- Koskinen, T. T., Yelle, R. V., Lavvas, P., & Lewis, N. K. 2010, *ApJ*, 723, 1, pp. 116-128 (2010)., 723, 116
- Kraus, A. L., & Hillenbrand, L. A. 2007, *AJ*, 134, 6, pp. 2340-2352 (2007)., 134, 2340
- Kraus, A. L., Shkolnik, E. L., Allers, K. N., & Liu, M. C. 2014, *AJ*, 147, 146
- Lammer, H., Lichtenegger, H. I., Kulikov, Y. N., et al. 2007, *Astrobiology*, 7, 185
- Lichtenegger, H., Lammer, H., Grießmeier, J.-M., et al. 2010, *Icarus*, 210, 1
- Lingam, M., & Loeb, A. 2017, eprint arXiv:1710.11134, arXiv:1710.11134
- Linsky, J. L., & Güdel, M. 2015, in *Astrophysics and Space Science Library*, Vol. 411, *Characterizing Stellar and Exoplanetary Environments*, ed. H. Lammer & M. Khodachenko, 3
- MacGregor, M. A., Weinberger, A. J., Wilner, D. J., Kowalski, A. F., & Cranmer, S. R. 2018, *ApJL*, 855, L2
- Malo, L., Doyon, R., Lafrenière, D., et al. 2013, *ApJ*, 762, 88

- Martin, D. C., Fanson, J., Schiminovich, D., et al. 2004, *ApJ*, 619, 1, pp. L1-L6., 619, L1
- Miles, B. E., & Shkolnik, E. L. 2017, *AJ*, 154, 2, 67, 19 pp. (2017)., 154, arXiv:1705.03583
- Montes, D., López-Santiago, J., Gálvez, M. C., et al. 2001, *MNRAS*, 328, 45
- Peacock, S., Barman, T., & Shkolnik, E. 2015, in AAS/Division for Planetary Sciences Meeting Abstracts, Vol. 47, AAS/Division for Planetary Sciences Meeting Abstracts #47, 404.06
- Pearson, K. 1895, Proceedings of the Royal Society of London Series I, 58, 240
- Pecaut, M. J., & Mamajek, E. E. 2013, *ApJS*, 208, 9
- Perryman, M. A. C., Brown, A. G. A., Lebreton, Y., et al. 1997, *A&A*, v.331, p.81-120 (1998), 331, 81
- Petigura, E. A., Howard, A. W., & Marcy, G. W. 2013, Proceedings of the National Academy of Sciences, vol. 110, 48, pp. 19273-19278, 110, 19273
- Price-Whelan, A. M., Sipócz, B. M., Günther, H. M., et al. 2018, *AJ*, 156, 123
- Ricker, G. R., Latham, D. W., Vanderspek, R. K., et al. 2009, American Astronomical Society, AAS Meeting #213, id.403.01; Bulletin of the American Astronomical Society, Vol. 41, p.193, 41, 193
- Ricker, G. R., Winn, J. N., Vanderspek, R., et al. 2014, Proceedings of the SPIE, 9143, id. 914320 15 pp. (2014)., 9143, arXiv:1406.0151
- Schaefer, L., & Fegley, B. 2010, *Icarus*, 208, 438
- Schmitt, J. H. M. M., Fleming, T. A., & Giampapa, M. S. 1995, *ApJ*, 450, 392
- Schneider, A. C., & Shkolnik, E. L. 2018, *AJ*, 155, 3, 122, 16 pp. (2018)., 155, arXiv:1801.06711
- Segura, A., Kasting, J. F., Meadows, V., et al. 2005, *Astrobiology*, 5, 6, pp. 706-725., 5, 706
- Segura, A., Krelove, K., Kasting, J. F., et al. 2003, *Astrobiology*, 3, 689
- Segura, A., Walkowicz, L., Meadows, V., Kasting, J., & Hawley, S. 2010, *Astrobiology*, 10, 7, pp. 751-771., 10, 751
- Shields, A. L., Ballard, S., & Johnson, J. A. 2016, *Physics Reports*, Vol. 663, p. 1â38 (2016), 663, 1
- Shkolnik, E. L., Allers, K. N., Kraus, A. L., Liu, M. C., & Flagg, L. 2017, *AJ*, 154, 2, 69, 23 pp. (2017)., 154, arXiv:1706.04556
- Shkolnik, E. L., & Barman, T. S. 2014, *AJ*, 148, 4, 64, 14 pp. (2014)., 148, arXiv:1407.1344
- Short, C. I., & Hauschildt, P. H. 2005, *ApJ*, 618, 926
- Spearman, C. 1904, *The American Journal of Psychology*, 15, 72
- Stelzer, B., Marino, A., Micela, G., López-Santiago, J., & Liefke, C. 2013, *MNRAS*, 431, 2063
- Tian, F., France, K., Linsky, J. L., Mauas, P. J. D., & Vieytes, M. C. 2014, *Earth and Planetary Science Letters*, 385, 22
- Truemper, J. 1982, *Advances in Space Research*, 2, 241
- van der Walt, S., Colbert, S. C., & Varoquaux, G. 2011, *Computing in Science and Engineering*, 13, 22
- van Leeuwen, F. 2009, *A&A*, 497, 209
- Voges, W., Aschenbach, B., Boller, T., et al. 1999, *A&A*, 349, 389
- Wang, J. J., Chen, L., Zhao, J. H., & Jiang, P. F. 1995, *A&AS*, 113, 419
- Zerkle, A. L., Claire, M. W., Domagal-Goldman, S. D., Farquhar, J., & Poulton, S. W. 2012, *Nature Geoscience*, 5, 359

Table 4. Observed flux densities F , fluxes f , and model photospheric flux densities σ of the stars used in this analysis.

Name ^a	RA	Dec	Mass	Dist.	F_J	σ_J	F_{NUV}	σ_{NUV}	F_{FUV}	σ_{FUV}	f_X
	2MASS	2MASS	[M_\odot]	[pc]	[μJy]	[μJy]	[μJy]	[μJy]	[μJy]	[μJy]	[$\text{erg cm}^{-2} \text{s}^{-1}$]
TW Hydra, 10 Myr											
Beta Pictoris, 23 Myr											
J00233468+2014282	00 23 34.6661	+20 14 28.637	0.71	63.15	3.53E+07	1.18E+07	7.73E+03 ± 4.20E+02	6.70E+01	— ± —	—	6.50E-11 ± 8.22E-12
J01373940+1835332	01 37 39.4039	+18 35 33.259	0.89	52.15	2.71E+07	3.24E+07	> 9.29E+03	6.79E+01	9.20E+04 ± 1.85E+03	5.13E-04	2.36E-10 ± 1.70E-11
J02273924+3058246	02 27 39.2543	+30 58 24.536	0.74	41.05	1.91E+07	1.29E+07	5.38E+03 ± 1.25E+02	4.76E+04 ± 1.02E+03	7.19E-03	1.60E-10 ± 9.06E-12	
J02303239+4342232	02 30 32.4110	+43 42 23.383	0.78	52.64	2.74E+07	1.44E+07	7.60E+03 ± 2.48E+02	5.28E+02 ± 6.08E+01	1.10E+02	4.01E+02 ± 9.80E+01	6.40E-11 ± 4.98E-12
J02304623+4343493	02 30 46.245	+43 43 49.55	0.72	52.84	9.75E+06	1.21E+07	1.20E+03 ± 1.10E+02	7.18E+01	8.41E-04	4.82E-11 ± 5.61E-12	
J02412558+0559181	02 41 25.88830	+05 59 18.4211	0.74	44.44	2.17E+07	1.29E+07	7.01E+03 ± 1.24E+02	8.24E+01	8.17E+02 ± 6.92E+01	1.10E-03	8.19E-11 ± 7.36E-12
CD-57 1054	05 00 47.1298	-57 15 25.453	0.52	26.90	1.68E+07	7.11E+06	2.60E+03 ± 6.68E+01	2.37E+01	4.22E+02 ± 4.68E+01	3.26E-05	3.19E-11 ± 1.56E-12
J05200029+0613036	05 20 00.291	+06 13 03.57	0.83	97.51	2.82E+07	1.71E+07	8.22E+03 ± 1.58E+03	1.92E+02	— ± —	—	5.55E-11 ± 1.12E-11
J05203182+0616115	05 20 31.8236	+06 16 11.589	0.83	97.26	3.02E+07	1.71E+07	7.59E+03 ± 1.80E+03	1.92E+02	9.75E-11 ± 1.39E-11	—	—
J06182824+7202416	06 18 28.2077	-72 02 41.447	0.72	39.26	1.21E+07	1.17E+04 ± 1.66E+02	7.18E+01	1.03E+03 ± 6.81E+01	8.88E-04	1.29E-10 ± 3.74E-12	
HIP 50156	10 14 19.17664	+21 04 29.054	0.52	23.40	1.29E+07	7.11E+06	2.30E+03 ± 8.14E+01	2.37E+01	4.31E+02 ± 6.82E+01	3.29E-05	2.11E-11 ± 1.60E-12
J10593879+2526138	10 59 38.6780	+25 26 13.712	0.78	21.32	1.61E+07	1.44E+07	7.50E+03 ± 1.10E+02	1.10E+02	1.16E+02 ± 2.28E+01	8.41E-04	— ± —
J141421.41-1521215	14 14 21.35665	-15 21 21.7551	0.78	28.96	1.43E+07	1.44E+07	4.29E+03 ± 9.54E+01	1.10E+02	8.51E+02 ± 9.19E+01	8.41E-04	4.81E-11 ± 3.15E-12
J16430128-1751274	16 43 01.2956	-17 54 27.539	0.52	71.05	1.34E+07	7.11E+06	3.34E+03 ± 2.41E+02	2.37E+01	< 1.19E+03	3.26E-05	4.00E-11 ± 8.69E-12
J19114467-2604085	19 11 44.670	-26 04 08.85	0.83	59.07	3.26E+07	1.71E+07	1.31E+04 ± 3.89E+02	7.05E+02 ± 4.84E+02	1.92E+01	5.63E-11 ± 9.46E-12	
J21100461-1920302	21 10 04.614	-19 20 30.120	0.74	34.27	7.96E+06	1.29E+07	7.67E+02 ± 4.75E+01	8.24E+01	2.89E+02 ± 4.75E+01	1.10E-03	4.71E-11 ± 4.28E-12
J21212448-6654573	21 21 24.48-6654573	-66 54 57.3758	0.93	31.98	2.52E+07	2.47E+07	1.80E+04 ± 1.37E+02	5.94E+02	7.02E+02 ± 4.61E+01	2.10E-02	4.43E-11 ± 4.31E-12
TYC 2211-1309-1	22 00 41.5840	+27 15 13.535	0.62	35.66	7.62E+06	9.14E+06	2.81E+03 ± 8.17E+01	3.90E+01	< 5.77E+01	1.63E-04	2.18E-11 ± 2.13E-12
J22424896-7142211	22 42 48.9342	-71 42 21.190	0.78	36.66	1.64E+07	1.44E+07	5.77E+03 ± 4.24E+01	1.10E+02	7.36E+02 ± 6.36E+01	8.41E-04	7.73E-11 ± 6.37E-12
BD-13 6424	23 32 34.8613	-12 15 51.476	0.62	27.37	1.25E+07	9.14E+06	2.11E+03 ± 8.80E+00	3.90E+01	3.15E+02 ± 4.62E+00	1.63E-04	3.83E-11 ± 2.81E-12
Columba, 42 Myr											
J03205070-1916086	03 20 50.70	-19 16 08.6	0.72	44.05	1.57E+07	1.10E+07	7.94E+03 ± 1.29E+02	1.73E+02	5.14E+02 ± 6.43E+01	5.79E-03	— ± —
J04105279-2231207	03 40 52.79	-22 31 20.7	0.86	80.57	2.00E+07	2.60E+07	1.68E+04 ± 4.61E+02	2.51E+03	< 1.65E+02	1.19E-01	— ± —
J04111512-5806479	04 11 15.12	-58 06 47.9	0.83	47.48	2.22E+07	2.18E+07	9.72E+03 ± 2.40E+02	2.34E+03	1.10E+02 ± 4.39E+01	1.17E-01	— ± —
J04323739-2736058	04 32 53.79	-27 36 05.8	0.72	56.02	1.06E+07	1.10E+07	1.96E+03 ± 1.25E+02	1.73E+02	< 9.58E+01	5.78E-03	— ± —
J04483160-1046496	04 48 31.60	-10 46 49.6	0.80	81.09	2.16E+07	1.78E+07	1.18E+04 ± 5.81E+02	5.22E+02	4.89E+02 ± 1.89E+02	1.77E-02	— ± —
J04590561-6323297	04 59 05.61	-63 23 29.7	0.72	86.99	5.52E+07	1.10E+07	8.35E+04 ± 1.06E+03	1.73E+02	6.01E+02 ± 1.73E+02	5.79E-03	1.40E-11 ± 3.15E-12
J05002547-2201400	05 00 28.47	-22 01 40.0	0.69	91.26	1.72E+07	9.62E+06	3.18E+03 ± 1.94E+02	6.15E+01	6.48E+02 ± 2.25E+02	9.19E-05	— ± —
J05275536-2743229	05 27 43.229	-27 43 22.9	0.86	51.05	5.04E+07	2.60E+07	1.04E+04 ± 1.04E+03	3.12E+02	< 3.12E+02	1.19E-01	— ± —
J055235004-0725278	05 52 39.04	-07 25 27.8	0.80	70.22	1.70E+07	1.78E+07	4.66E+03 ± 6.12E+02	5.22E+02	— ± —	— ± —	
J06772781-3547244	06 27 27.81	-35 47 24.4	0.77	97.23	1.60E+07	1.46E+07	2.56E+03 ± 4.74E+02	3.45E+01	< 5.80E+02	5.80E-03	— ± —
HIP 30034 A	06 19 12.91	-58 03 15.6	0.88	50.12	3.73E+07	3.03E+07	5.46E+04 ± 5.53E+02	9.78E+03	1.45E+03 ± 1.54E+02	6.68E-01	1.04E-10 ± 3.80E-12
Tucana Horologium, 45 Myr											
HIP 1910	00 24 08.98105	-62 11 04.2982	0.69	44.23	1.38E+07	9.69E+06	2.83E+03 ± 1.47E+02	6.85E+01	6.39E+02 ± 1.11E+02	4.60E-04	2.53E-11 ± 7.10E-12
C/T Tuc	00 25 14.6619	-61 30 48.251	0.72	44.16	1.11E+07	1.13E+07	2.23E+03 ± 9.59E+01	1.92E+02	2.79E+02 ± 5.23E+01	6.15E-03	— ± —
HD 3221	00 34 51.2018	-61 54 58.127	0.77	44.50	3.67E+07	1.53E+07	1.71E+03 ± 2.65E+02	1.29E+02	1.57E+03 ± 1.41E+02	6.44E-04	8.03E-11 ± 9.93E-12
CD-78 24	00 42 20.3154	-77 47 39.755	0.80	49.76	2.03E+07	1.89E+07	1.13E+04 ± 2.08E+02	8.44E+02	< 1.01E+02	3.11E-02	4.81E-02

Table 4 *continued*

Table 4 (continued)

Name ^a	RA	Dec	Mass	Dist.	F_J	σ_J	F_{NUV}	σ_{NUV}	F_{FUV}	σ_{FUV}	f_X
	2MASS	2MASS	[M_\odot]	[pc]	[μJy]	[μJy]	[μJy]	[μJy]	[μJy]	[μJy]	[erg cm $^{-2}$ s $^{-1}$]
J02000918-8025009	02 00 9.18	-80 25 00.9	0.80	74.65	2.98E+07	1.89E+07	1.09E+04 ± 2.99E+02	8.44E+02	< 1.79E+02	3.11E-02	— ± —
CD-60 416	02 07 33.2079	-59 40 21.054	0.80	45.46	1.54E+07	1.89E+07	< 7.31E+01	8.04E+02 ± 1.17E+02	3.11E-02	8.13E-12	8.31E-12
J02105338-4603588	02 10 50.38	-46 03 58.8	0.80	81.78	2.05E+07	1.89E+07	1.74E+04 ± 1.67E+02	8.44E+02	9.65E+02 ± 1.78E+02	3.11E-02	8.09E-11 ± 1.13E-11
J02372562-4912033	02 37 25.614	-49 12 03.32	0.60	50.68	6.48E+06	6.37E+06	1.75E+02 ± 4.83E+01	3.26E+01	< 7.80E+01	2.02E-04	— ± —
CD-53 544	02 41 46.8340	-52 59 52.376	0.77	43.81	2.84E+07	1.53E+07	8.59E+03 ± 1.90E+02	1.29E+02	1.35E+03 ± 1.08E+02	6.44E-04	1.29E-10 ± 6.36E-12
CD-58 553	02 42 33.0232	-57 39 36.812	0.77	49.72	1.48E+07	1.53E+07	3.86E+03 ± 1.29E+02	1.29E+02	5.54E+02 ± 8.40E+01	6.44E-04	2.11E-11 ± 4.91E-12
CD-35 1167	03 19 08.6657	-35 07 00.296	0.77	45.56	1.23E+07	1.53E+07	2.32E+03 ± 9.26E+01	1.29E+02	2.97E+02 ± 5.79E+01	6.44E-04	1.85E-11 ± 4.31E-12
CD-44 1173	03 31 55.6411	-43 59 13.549	0.60	45.28	1.56E+07	6.37E+06	3.60E+03 ± 4.66E+01	3.26E+01	4.75E+02 ± 8.24E+01	3.75E-04	3.75E-11 ± 4.58E-12
CD-44 1173	03 31 55.6411	-43 59 13.549	0.60	45.28	1.56E+07	6.37E+06	3.60E+03 ± 4.66E+01	3.26E+01	4.75E+02 ± 8.24E+01	3.02E-04	— ± —
J0400382-2902165	04 00 03.82	-29 02 16.5	0.77	49.38	2.54E+07	1.53E+07	1.45E+04 ± 3.59E+02	1.29E+02	1.90E+03 ± 2.03E+02	6.44E-04	1.17E-10 ± 7.52E-12
J0400395-2902280	04 00 03.95	-29 02 28.0	0.80	48.82	1.85E+07	1.89E+07	9.19E+03 ± 2.84E+02	8.44E+02	9.44E+02 ± 1.43E+02	3.11E-02	1.14E-10 ± 7.35E-12
J04021648-1522297	04 02 16.48	-15 21 29.7	0.83	54.84	2.45E+07	2.35E+07	2.83E+04 ± 6.16E+02	3.50E+03	1.36E+03 ± 2.02E+02	1.71E-01	5.61E-11 ± 6.44E-12
J04480066-5041255	04 48 00.6676	-50 41 25.663	0.72	59.60	1.81E+07	3.24E+03	2.37E+02 ± 1.39E+02	5.57E+02	6.11E+02 ± 5.45E+02	5.22E-11 ± 5.45E-12	
J05332558-5117131	05 33 25.58	-51 17 13.1	0.77	53.95	1.08E+07	1.53E+07	2.48E+03 ± 5.88E+01	1.29E+01	2.24E+02 ± 1.16E+02	6.44E-04	1.32E-11 ± 2.32E-12
HIP 107345	21 44 30.12081	-60 58 38.8797	0.69	46.36	9.69E+06	2.42E+03	6.83E+01	6.85E+01	3.74E+02 ± 1.518E+01	4.60E-04	2.33E-11 ± 3.78E-12
HIP 107345	21 44 30.12081	-60 58 38.8797	0.69	46.36	1.08E+07	9.69E+06	2.42E+03 ± 6.83E+01	6.85E+01	3.74E+02 ± 5.18E+01	4.60E-04	— ± —
J22021626-4210329	22 02 16.26	-42 10 33.0	0.52	44.35	8.44E+06	4.89E+06	1.52E+03 ± 5.85E+01	1.87E+01	3.52E+02 ± 5.09E+01	4.11E-05	2.78E-11 ± 4.05E-12
J23261063-7323498	23 26 10.7051	-73 23 49.895	0.66	46.29	9.94E+06	8.36E+06	2.43E+03 ± 1.58E+02	3.18E+01	7.65E+02 ± 1.34E+02	7.81E-04	4.19E-11 ± 5.85E-12
J23474694-6517249	23 47 46.95	-65 17 24.9	0.52	45.39	7.53E+06	4.89E+06	1.46E+03 ± 1.14E+02	1.87E+01	2.63E+02 ± 8.19E+01	4.11E-05	1.49E-11 ± 2.83E-12
J23585674-8339423	23 58 56.74	-83 39 42.3	0.72	55.63	1.11E+07	1.13E+07	2.09E+03 ± 4.60E+01	1.92E+02	1.79E+02 ± 7.47E+01	6.15E-03	— ± —
AB Doradus, 150 Myr											
HIP 5191	01 06 26.14	-14 17 46.8	0.89	45.43	2.26E+07	2.68E+07	2.18E+04 ± 4.19E+02	1.31E+04	1.67E+02 ± 6.05E+01	9.12E-01	2.23E-11 ± 3.73E-12
HIP 40272	02 12 15.35	+23 57 29.8	0.61	32.08	1.08E+07	6.13E+06	> 5.82E+04	6.79E+01	9.74E+02 ± 9.02E+01	9.12E-01	1.49E-11 ± 2.84E-12
HIP 12635	02 42 20.94	+38 37 21.2	0.75	49.33	1.73E+07	1.29E+07	< 3.05E+01	5.87E+02	4.33E+02 ± 3.09B+01	2.37E-02	3.34E-11 ± 3.83E-12
HIP 25647	05 28 44.84	-65 26 55.1	0.59	15.31	1.02E+07	5.30E+06	> 6.44E+04	5.70E+01	2.37E+03 ± 1.89E+01	9.12E-01	1.28E-10 ± 8.85E-13
HIP 26369	05 36 55.09	-47 37 48.1	0.59	24.64	1.02E+07	5.30E+06	< 1.33E+01	5.70E+01	4.94E+02 ± 5.58E+01	1.19E-03	9.46E-11 ± 2.32E-12
HIP 26373	05 36 56.85	-47 57 52.8	0.61	24.63	8.37E+06	6.13E+06	> 1.28E+04	6.79E+01	1.76E+03 ± 1.03B+02	3.03E+00	9.48E-11 ± 2.31E-12
HIP 31878	06 39 50.03	-61 28 41.7	0.59	22.24	9.47E+06	5.30E+06	1.42E+03 ± 3.36E+01	1.20E+02	1.32E+02 ± 1.54E+01	5.91E-12	1.19E-11 ± 5.40E-13
HIP 76768	15 40 28.40	-18 41 46.0	0.80	38.45	1.88E+07	1.66E+07	6.30E+03 ± 1.42E+02	1.78E+03	4.28E+02 ± 9.46E+01	8.81E-02	5.25E-11 ± 3.98E-12
HIP 106231	21 31 01.71	+23 20 07.4	0.57	24.25	1.39E+07	4.76E+06	7.59E+03 ± 1.88E+02	4.38E+01	— ± —	4.37E-11 ± 2.47E-12	
HIP 113597	23 00 27.91	-26 18 43.1	0.57	31.77	2.44E+07	4.76E+06	3.61E+03 ± 5.37E+01	4.38E+01	3.61E+02 ± 4.20B+01	7.61E-04	2.33E-11 ± 4.39E-12
HIP 118008	23 56 10.67	-39 03 08.6	0.80	21.93	1.91E+07	1.66E+07	2.34E+03 ± 9.37E+01	1.78E+03	1.38E+02 ± 1.81E+01	8.81E-02	5.26E-12 ± 1.40E-12
Ursa Majoris, 414 Myr											
HIP 35628	07 21 06.7319	+67 39 42.608	0.92	25.87	2.06E+07	3.15E+07	1.80E+04 ± 1.70E+02	3.05E+04	1.15E+02 ± 3.21E+01	2.57E+00	4.02E-12 ± 7.66E-13
HIP 37349	07 39 59.3286	-03 35 51.027	0.86	14.10	2.01E+07	2.31E+07	— ± —	—	1.05E+02 ± 1.08E+01	4.15E-01	2.33E-12 ± 2.84E-13
HIP 56337	11 32 57.0557	+52 31 25.554	0.75	46.02	3.12E+07	3.03E+07	> 2.55E+05	9.29E+01	2.69E+02 ± 1.90E+01	2.57E+00	— ± —
HIP 71395	14 36 00.56029	+09 44 47.4632	0.80	16.34	2.09E+07	1.74E+07	9.21E+03 ± 1.01E+02	1.87E+03	1.32E+02 ± 1.12E+01	9.08E-02	2.66E-12 ± 3.93E-13
HIP 74702	15 15 59.1669	+00 47 47.46399	0.86	15.81	2.73E+07	2.71E+07	> 5.16E+04	1.34E+04	2.32E+02 ± 7.12E+00	5.57E+00	1.12E-12 ± 1.99E-13
HIP 92919	18 55 53 22506	+23 33 23.9349	0.83	21.35	2.15E+07	2.27E+07	> 1.55E+04	5.21E+03	1.15E+03 ± 4.16E+01	2.57E+00	— ± —
HIP 104383	21 08 45.46901	-04 25 36.9339	0.65	23.94	1.27E+07	7.53E+06	2.34E+03 ± 3.72E+01	1.09E+02	1.51E+02 ± 1.52B+01	3.01E-03	2.91E-11 ± 1.80E-12
Praesepse, 600 Myr											
C1* NGC 2632 JC 107	08 37 36.243	+19 15 54.30	0.71	189.05	1.53E+07	1.07E+07	3.43E+03 ± 1.07E+02	2.71E+02	< 1.70E+03	1.00E-02	— ± —
C1* NGC 2632 KW 184	08 39 28.586	+19 28 25.13	0.92	184.62	5.26E+07	3.21E+07	— ± —	—	3.99E+02 ± 1.03E+02	2.60E+00	— ± —
C1* NGC 2632 JC 163	08 39 29.407	+19 47 11.88	0.80	199.62	3.22E+07	1.74E+07	— ± —	—	6.25E+02 ± 1.75E+02	8.94E-02	— ± —
C1* NGC 2632 JC 208	08 40 26.241	+19 13 09.92	0.80	186.89	2.04E+07	1.74E+07	9.44E+03 ± 1.41E+03	1.85E+03	< 1.41E+03	8.94E-02	— ± —
C1* NGC 2632 JC 215	08 40 33.473	+19 38 00.97	0.89	187.36	2.92E+07	2.77E+07	— ± —	—	3.16E+02 ± 7.75E+01	1.02E+00	— ± —

Table 4 continued

Table 4 (continued)

Name ^a	RA	Dec	Mass	Dist.	F_J	σ_J	F_{NUV}	σ_{NUV}	F_{FUV}	σ_{FUV}	f_X
	2MASS	2MASS	[M $_\odot$]	[pc]	[μ Jy]	[μ Jy]	[μ Jy]	[μ Jy]	[μ Jy]	[μ Jy]	[erg cm $^{-2}$ s $^{-1}$]
Cl* NGC 2632 JS 395	08 40 54.879	+19 56 06.72	0.89	181.52	3.03E+07	2.77E+07	—	—	1.51E+03	\pm 2.29E+02	1.02E+00
Cl* NGC 2632 JC 278	08 42 11.492	+19 16 37.36	0.89	188.93	3.10E+07	2.77E+07	< 1.79E+03	1.49E+04	4.62E+02	\pm 1.67E+02	1.02E+00
Cl* NGC 2632 W1JP 899	08 43 08.226	+19 42 47.55	0.75	186.38	1.68E+07	1.33E+07	—	—	6.90E+02	\pm 2.82E+02	2.35E-02
J08431522+20034361	08 43 15.219	+20 03 56.062	0.77	185.06	1.56E+07	1.46E+07	4.40E+03	1.10E+03	2.08E+03	\pm 2.54E+02	3.51E-02
J08364182+20244400	08 36 41.817	+20 24 39.942	0.81	194.04	2.02E+07	1.85E+07	1.37E+04	\pm 2.03E+03	2.42E+03	< 2.33E+03	1.27E-01
J08414369+1957438	08 41 43.681	+19 57 43.075	0.89	192.83	2.93E+07	2.71E+07	—	—	4.17E+02	\pm 9.35E+01	8.86E-01
J08394445+2057207	08 39 34.445	+20 57 20.602	0.75	187.25	1.48E+07	1.32E+07	1.42E+03	6.67E+02	5.70E+02	< 2.84E+03	2.26E-02
J08373624+19155433	08 37 36.240	+19 15 54.230	0.75	189.05	5.05E+07	3.43E+03	1.07E+03	5.53E+02	6.14E+02	< 1.70E+03	2.20E-02
J08424848+2034245	08 42 48.464	+20 34 24.315	0.88	256.46	2.65E+07	4.10E+04	+ 4.18E+03	1.30E+04	3.37E+03	8.56E-01	—
J08384610+2034364	08 38 46.098	+20 34 36.375	0.87	188.38	2.65E+07	2.51E+07	2.29E+04	\pm 2.13E+03	9.24E+03	4.96E+02	\pm 1.69E+02
J08355387+1855475	08 35 33.867	+18 55 47.478	0.61	184.96	6.72E+06	5.76E+06	3.70E+02	\pm 1.33E+02	6.21E+01	< 2.91E+02	1.30E-03
J08421665+2005325	08 42 16.640	+20 05 32.431	0.69	189.35	1.14E+07	9.26E+06	—	—	4.46E+02	\pm 1.48E+02	5.98E-03
J08430823+1942476	08 43 08.217	+19 42 47.512	0.77	186.38	1.68E+07	1.49E+07	—	—	6.90E+02	\pm 2.82E+02	3.9E-02
J08364270+1853429	08 36 42.685	+18 53 42.784	0.72	185.44	1.12E+07	1.14E+07	4.14E+03	5.50E+02	3.39E+02	< 2.85E+02	1.30E-02
J08423701+2008319	08 42 36.994	+20 08 31.804	0.72	186.80	1.23E+07	1.10E+07	< 1.87E+03	2.96E+02	1.65E+03	\pm 2.12E+02	1.11E-02
J08443871+2017260	08 44 48.702	+20 17 25.954	0.82	186.49	2.05E+07	1.89E+07	7.161E+03	\pm 1.43E+03	2.66E+03	< 1.71E+03	1.45E-01
J08444076+2011371	08 44 40.744	+20 11 37.053	0.67	185.56	8.45E+06	8.45E+06	< 1.72E+03	1.44E+02	5.09E+02	\pm 1.29E+02	4.31E-03
J0840531+1834593	08 40 55.305	+18 34 59.102	0.66	188.21	9.60E+06	7.91E+06	2.34E+03	\pm 9.63E+02	1.23E+02	1.06E+03	3.46E-03
J08341024+1948178	08 34 10.231	+19 48 17.762	0.69	186.78	9.26E+06	9.26E+06	1.56E+03	\pm 2.09E+02	8.83E+02	< 2.17E+02	5.98E-03
J08362639+1911294	08 36 26.683	+19 11 29.295	0.89	182.69	2.63E+07	2.71E+07	2.16E+04	\pm 1.93E+03	1.35E+04	< 1.47E+03	8.39E-01
J08342412+1947362	08 34 37.216	+19 47 36.248	0.78	192.73	1.84E+07	1.58E+07	4.79E+03	\pm 6.62E+02	1.23E+03	< 2.39E+02	2.8E-02
J0843181+1954490	08 43 51.804	+19 54 48.949	0.69	186.39	1.04E+07	9.41E+06	1.24E+03	\pm 6.00E+02	1.91E+02	—	—
J08355988+1931321	08 35 59.868	+19 31 31.929	0.80	174.61	1.59E+07	1.73E+07	4.01E+03	\pm 1.08E+03	1.81E+03	< 1.40E+03	8.68E-02
J08422009+1909058	08 42 20.079	+19 09 05.691	0.76	188.15	1.56E+07	1.43E+07	6.78E+03	\pm 2.10E+03	8.03E+02	—	—
J08384723+2010337	08 38 57.216	+20 10 53.562	0.76	177.08	1.39E+07	< 1.88E+07	4.79E+03	\pm 6.62E+02	7.09E+02	4.78E+02	\pm 1.12E+02
J08375180+1924538	08 37 51.800	+19 24 53.708	0.78	213.49	2.45E+07	1.60E+07	1.24E+03	\pm 6.00E+02	1.91E+02	< 2.10E+03	5.64E-02
J08360865+1844509	08 36 08.638	+18 44 50.902	0.63	183.35	7.67E+06	6.64E+06	5.61E+02	\pm 2.54E+02	8.38E+01	< 2.86E+02	2.03E-03
J08441707+1844119	08 44 17.065	+18 44 11.756	0.88	187.20	2.76E+07	2.69E+07	2.80E+04	\pm 2.26E+03	1.30E+04	< 1.65E+03	8.56E-01
J08434648+1853369	08 43 54.667	+18 53 36.920	0.84	187.50	2.31E+07	2.18E+07	1.23E+04	\pm 1.57E+03	4.91E+03	< 1.75E+03	2.88E-01
J08441324+1849114	08 44 13.234	+18 49 11.380	0.70	197.84	1.25E+07	9.84E+06	2.30E+03	\pm 9.79E+02	2.16E+02	< 1.90E+03	7.46E-03
J08435106+1832548	08 43 31.047	+18 32 54.711	0.75	169.14	2.45E+07	1.60E+07	7.88E+03	\pm 1.95E+03	1.30E+03	< 2.10E+03	5.64E-02
J08360865+1844509	08 36 08.638	+18 44 50.902	0.63	183.35	7.67E+06	6.64E+06	5.61E+02	\pm 2.54E+02	8.38E+01	< 2.86E+02	2.03E-03
J08441707+1844119	08 44 17.065	+18 44 11.756	0.88	187.20	2.76E+07	2.69E+07	2.80E+04	\pm 2.26E+03	1.30E+04	< 1.65E+03	8.56E-01
J08373346+1910412	08 37 03.449	+19 10 41.134	0.75	176.32	1.32E+07	1.36E+07	9.27E+03	\pm 2.55E+03	6.59E+02	< 1.45E+03	2.61E-02
J08333290+1840575	08 33 02.889	+18 40 57.464	0.77	186.79	1.63E+07	1.47E+07	3.15E+03	\pm 2.00E+02	9.06E+02	< 2.93E+02	3.66E-02
J08461010+1931439	08 46 10.096	+19 31 43.813	0.62	187.58	7.16E+06	6.07E+06	2.76E+03	\pm 3.29E+02	6.95E+01	1.30E+03	1.55E-03
J08463304+1854242	08 46 33.032	+18 54 24.188	0.79	187.03	1.68E+07	1.60E+07	1.99E+03	\pm 7.73E+02	1.31E+03	< 1.74E+03	5.74E-02
J08322224+1958359	08 32 52.225	+19 58 35.900	0.80	187.00	1.94E+07	1.75E+07	6.52E+03	\pm 2.60E+02	1.92E+03	< 1.99E+02	9.31E-02
J08433234+1910412	08 43 32.413	+20 04 48.327	0.78	180.73	1.61E+07	1.58E+07	3.45E+03	\pm 2.05E+02	1.25E+03	< 1.45E+03	2.61E-02
J08434357+1904332	08 43 43.557	+19 04 33.175	0.74	196.46	1.64E+07	1.25E+07	4.50E+03	\pm 2.05E+02	4.63E+02	< 2.17E+03	1.83E-02
J0830102+1921089	08 30 51.018	+19 21 08.838	0.65	182.08	8.21E+06	7.36E+06	4.22E+02	\pm 1.04E+02	1.04E+02	< 2.02E+02	2.75E-03
J0839752+1810134	08 39 37.514	+18 10 13.393	0.89	184.29	1.14E+07	1.07E+07	—	—	—	< 2.83E+02	1.06E+00
J0836164+1904351	08 36 51.632	+19 04 35.014	0.72	187.35	1.31E+07	1.13E+07	1.78E+03	\pm 9.53E+02	3.20E+02	< 1.64E+03	1.22E-02
J08322342+2004483	08 32 33.413	+20 04 48.327	0.78	180.73	1.61E+07	1.58E+07	3.45E+03	\pm 2.05E+02	1.25E+03	< 1.83E+02	5.34E-02
J08434357+1904332	08 43 43.557	+19 04 33.175	0.74	196.46	1.64E+07	1.25E+07	4.50E+03	\pm 2.05E+02	4.63E+02	< 2.17E+03	1.83E-02
J08461010+1931439	08 46 10.096	+19 31 43.813	0.62	187.58	7.16E+06	6.07E+06	2.76E+03	\pm 3.29E+02	6.95E+01	1.30E+03	1.55E-03
J08373375+1840025	08 37 03.742	+18 40 02.510	0.71	187.60	7.12E+06	6.07E+06	2.76E+03	\pm 3.29E+02	6.95E+01	< 2.83E+02	1.02E-02
J08492676+1831196	08 49 26.759	+18 31 19.542	0.61	187.60	7.12E+06	6.07E+06	2.76E+03	\pm 3.29E+02	6.95E+01	< 1.52E+02	1.43E-03
J08413600+1904332	08 41 35.991	+19 06 25.488	0.69	186.00	1.10E+07	9.37E+06	1.82E+03	\pm 7.22E+02	1.89E+02	< 1.40E+03	6.25E-03
J08343646+1823531	08 34 36.460	+18 23 53.037	0.61	193.09	5.69E+06	5.69E+06	9.64E+02	\pm 1.76E+02	6.03E+01	< 2.77E+02	1.24E-03
J08463012+2101129	08 46 50.116	+21 01 12.799	0.81	180.08	1.81E+07	1.79E+07	6.32E+03	\pm 1.39E+03	2.12E+03	< 1.81E+03	1.07E-01
J083331763+1925505	08 33 17.614	+19 25 50.458	0.72	185.95	1.28E+07	1.12E+07	1.63E+03	\pm 1.62E+02	3.14E+02	< 2.01E+02	1.19E-02
J08363375+1829451	08 36 53.737	+18 29 45.092	0.69	187.26	1.20E+07	9.74E+06	1.49E+03	\pm 3.08E+02	2.10E+02	< 2.74E+02	7.21E-03

Table 4 continued

THE UV AND X-RAY EVOLUTION OF K STARS

Table 4 (continued)

Name ^a	RA	Dec	Mass	Dist.	F _J	σ_J	F _{NUV}	σ_{NUV}	F _{FUV}	σ_{FUV}	f _X
	2MASS	2MASS	[M _⊙]	[pc]	[μJy]	[μJy]	[μJy]	[μJy]	[μJy]	[μJy]	[erg cm ⁻² s ⁻¹]
<hr/>											
J08383724+1901161	08 38 37.229	+19 01 16.046	0.79	187.26	1.61E+07	1.62E+07	1.54E+03 ± 9.90E+02	1.37E+03	< 1.95E+03	6.03E-02	— ± —
J08325566+1843582	08 32 55.636	+18 43 58.148	0.79	188.39	1.83E+07	1.64E+07	6.00E+03 ± 2.71E+02	1.47E+03	< 2.93E+02	6.60E-02	— ± —
J08330746+2007483	08 33 07.456	+20 07 48.244	0.70	186.80	1.18E+07	1.01E+07	2.04E+03 ± 1.71E+02	2.29E+02	3.72E+02 ± 1.07E+02	8.08E-03	— ± —
J08384973+1815572	08 38 49.727	+18 15 57.106	0.85	187.64	2.41E+07	2.23E+07	1.53E+04 ± 2.69E+02	5.44E-03	< 2.92E+02	3.21E-01	— ± —
J08461382+2051248	08 46 13.809	+20 51 24.753	0.72	176.01	1.07E+07	1.12E+07	1.44E+03 ± 5.76E+02	3.17E+02	— ± —	—	— ± —
J08365411+1845248	08 36 54.103	+18 45 24.706	0.83	181.70	2.09E+07	2.00E+07	1.69E+04 ± 8.79E+02	3.41E+03	< 3.21E+02	1.93E-01	— ± —
J08344714+1801162	08 34 47.138	+18 01 16.161	0.73	192.07	1.44E+07	1.17E+07	2.68E+03 ± 2.71E+02	3.65E+02	< 2.95E+02	1.42E-02	— ± —
<hr/>											
HIP 13806	02 57 46.6727	+29 39 41.268	0.92	41.53	3.06E+07	3.21E+07	3.57E+04 ± 5.03E+02	3.11E+04	1.68E+02 ± 5.77E+01	2.60E+00	5.39E-12 ± 1.20E-12
HIP 13976	03 00 02.81119	+07 44 59.119	0.80	23.79	2.67E+07	1.74E+07	1.77E+04 ± 2.19E+02	1.85E+03	< 1.12E+01	8.94E-02	2.93E-12 ± 7.19E-13
HIP 15374	03 18 15.10184	+09 14 42.5704	0.71	61.51	1.08E+07	1.07E+07	—	—	< 1.31E+02	1.00E-02	— ± —
HIP 15563	03 20 28.1951	+08 27 16.025	0.71	31.77	1.54E+07	1.07E+07	3.18E+03 ± 8.83E+01	2.71E+02	1.75E+02 ± 3.32E+01	—	— ± —
HIP 15720	03 22 28.1400	+27 09 21.792	0.62	31.75	8.06E+06	6.24E+06	5.92E+02 ± 5.19E+01	7.38E-01	< 5.27E+01	1.69E-03	— ± —
HIP 16548	03 33 05.2980	+04 57 29.240	0.71	54.99	8.83E+06	1.07E+07	8.34E+02 ± 1.24E+02	2.71E+02	< 1.63E+02	1.00E-02	— ± —
HIP 17766	03 48 11.8636	+07 08 46.477	0.62	36.33	1.04E+07	6.24E+06	7.67E+02 ± 5.63E+01	7.38E+01	< 9.64E+01	1.69E-03	— ± —
HIP 17962	03 50 24.9669	+17 14 47.331	0.83	47.72	> 2.27E+07	> 2.34E+07	> 4.20E+04	> 5.21E+03	> 1.65E+05	2.45E-01	1.70E-10 ± 7.35E-12
HD 283044	03 52 41.0090	+25 48 15.980	0.62	44.46	1.04E+07	6.24E+06	1.23E+03 ± 1.44E+02	7.38E+01	— ± —	—	— ± —
HIP 18327	03 55 06.5014	+16 59 54.920	0.92	40.98	2.90E+07	3.21E+07	2.75E+04 ± 6.62E+02	3.11E+04	< 2.51E+02	2.60E+00	5.18E-12 ± 1.76E-12
HIP 18946	04 03 39.0405	+19 27 18.046	0.86	48.04	1.92E+07	2.38E+07	5.85E+03 ± 4.41E+01	7.28E+03	< 1.69E+02	4.32E-01	— ± —
HIP 19263	04 07 43.1990	+16 31 07.644	0.92	46.56	1.98E+07	3.21E+07	8.15E+03 ± 1.07E+02	3.11E+04	3.05E+03 ± 2.91E+02	2.60E+00	— ± —
HIP 19441	04 09 49.3492	+09 18 19.771	0.75	36.01	1.42E+07	1.33E+07	2.23E+03 ± 9.05E+01	5.92E+02	< 8.39E+01	2.35E-02	— ± —
V* V1313 Tau	04 18 10.7920	+23 17 04.765	0.92	54.01	4.30E+07	4.30E+07	4.07E+03 ± 1.44E+02	3.11E+04	2.30E+03 ± 9.82E+01	1.29E-10 ± 8.25E-12	— ± —
HD 283052	04 18 19.2717	+16 20 17.395	0.92	45.18	3.21E+07	3.21E+07	1.29E+04 ± 7.83E+01	3.11E+04	2.30E+03 ± 9.82E+01	2.60E+00	— ± —
HD 285773	04 29 31.6064	+17 53 35.459	0.92	45.79	3.27E+07	3.21E+07	4.65E+04 ± 6.57E+02	3.11E+04	—	—	— ± —
HD 28462	04 29 57.7280	+16 40 22.226	0.89	45.67	2.98E+07	2.77E+07	3.92E+04 ± 3.38E+02	1.49E+04	1.76E+02 ± 4.45E+01	1.02E+00	— ± —
HD 29159	04 36 05.2667	+15 41 02.418	0.92	50.22	2.89E+07	3.21E+07	3.61E+04 ± 7.86E+01	3.11E+04	2.67E+02 ± 1.88E+01	2.60E+00	— ± —
HD 30505	04 49 03.5240	+18 38 28.480	0.89	45.73	3.38E+07	2.77E+07	4.60E+04 ± 4.68E+02	1.49E+04	2.02E+02 ± 7.24E+01	1.02E+00	8.06E-12 ± 2.47E-12
HIP 23312	05 00 48.8664	+04 53 59.203	0.86	52.06	2.46E+07	1.86E+07	1.86E+04 ± 1.25E+02	4.23E+02 ± 1.46E+02	4.32E-01	— ± —	
HD 32347	05 03 07.6575	+13 43 50.413	0.92	53.76	4.09E+07	3.21E+07	9.39E+04 ± 8.12E+02	3.11E+04	4.10E+02 ± 1.18E+02	2.65E-12 ± 9.40E-13	— ± —
HD 240648	05 06 17.9892	+17 48 59.098	0.79	53.75	2.00E+07	1.82E+07	> 1.10E+04	—	< 4.42E+02	1.02E+00	2.23E-12 ± 2.16E-12
J04053965+1756156	04 05 39.596	+17 56 16.000	0.89	45.81	2.66E+07	2.77E+07	2.78E+04 ± 1.22E+02	1.49E+04	2.48E+02 ± 6.18E+01	1.02E+00	4.97E-12 ± 2.28E-12
J04083620+2346071	04 08 36.208	+23 46 06.396	0.89	47.52	2.63E+07	2.77E+07	2.06E+04 ± 2.60E+02	1.49E+04	2.70E+02 ± 7.00E+01	1.02E+00	3.22E-12 ± 1.45E-12
J0418.926+1605181	04 18 19.199	+16 05 18.198	0.86	45.18	2.29E+07	2.38E+07	1.29E+04 ± 7.83E+01	7.28E+03	1.77E+02 ± 3.60E+01	4.32E-01	— ± —
J04431568+1744540	04 46 49.395	+17 44 54.261	0.89	48.09	2.80E+07	4.09E+07	3.21E+04 ± 1.0E+04	7.01E+03	—	—	— ± —
J04431568+17445408	04 46 49.388	+17 44 59.088	0.87	45.93	2.12E+07	2.51E+07	1.01E+04 ± 7.01E+01	9.19E+03	3.16E+02 ± 8.45E+01	5.60E-01	1.26E-11 ± 2.63E-12
J04074319+1631076	04 07 43.124	+16 31 07.862	0.82	46.56	1.98E+07	1.93E+07	8.15E+03 ± 1.07E+02	2.91E+03	3.05E+03 ± 2.91E+02	1.60E-01	— ± —
J04094935+0918197	04 09 49.257	+09 18 19.817	0.75	36.01	1.41E+07	1.33E+07	2.23E+03 ± 9.05E+01	5.92E+02	< 8.39E+01	2.33E-02	— ± —
J04035902+1927180	04 03 38.964	+19 27 18.338	0.83	48.04	1.92E+07	2.04E+07	5.85E+03 ± 4.41E+01	3.67E+03	< 1.69E+02	2.09E-01	— ± —
J04250024+1659057	04 25 00.18s	+16 59 05.784	0.82	54.70	1.92E+07	1.93E+07	— ± —	—	< 4.86E+01	1.60E-01	— ± —
J04070122+1520062	04 07 01.150	+15 20 06.28s	0.77	45.09	1.46E+07	1.48E+07	2.57E+03 ± 7.94E+01	9.26E+02	—	—	— ± —
J04471178+2609009	04 47 41.726	+26 09 01.555	0.65	47.61	1.53E+07	7.53E+06	1.71E+03 ± 3.68E+01	1.10E+02	< 1.22E+02	2.95E-03	— ± —
J04333716+2109030	04 33 37.112	+21 09 03.468	0.75	43.80	1.30E+07	1.33E+07	1.58E+03 ± 7.74E+01	5.92E+02	< 1.15E+02	2.33E-02	— ± —
J04145191+1303178	04 14 51.864	+13 03 17.996	0.80	44.55	1.32E+07	1.74E+07	1.97E+03 ± 4.09E+01	1.85E+03	< 1.74E+02	8.94E-02	7.50E-12 ± 2.23E-12
J04500069+1624436	04 50 00.700	+16 24 43.488	0.76	49.40	1.57E+07	1.40E+07	3.22E+03 ± 5.52E+01	7.38E+02	< 1.50E+02	2.93E-02	— ± —
J04334192+1903054	04 33 41.865	+19 00 50.819	0.74	47.80	1.40E+07	1.26E+07	2.33E+03 ± 1.79E+02	4.78E+02	— ± —	—	— ± —
J04175212+1901478	04 17 25.14s	+19 01 47.388	0.74	47.86	1.33E+07	1.26E+07	1.77E+03 ± 3.89E+01	4.78E+02	< 9.74E+01	1.89E-02	— ± —
J04081110+1652229	04 08 11.020	+16 52 23.304	0.67	40.13	8.00E+06	8.48E+06	6.58E+02 ± 6.15E+00	1.45E+02	6.39E+01 ± 1.80E+01	4.33E-03	— ± —

Table 4 continued

Table 4 (continued)

Name ^a	RA	Dec	Mass	Dist.	F_J	σ_J	F_{NUV}	σ_{NUV}	F_{FUV}	σ_{FUV}	f_X
	2MASS	2MASS	[M _⊙]	[pc]	[μJy]	[μJy]	[μJy]	[μJy]	[μJy]	[μJy]	[erg cm ⁻² s ⁻¹]
J04052565+1926316	04 05 25.595	+19 26 32.032	0.68	47.30	9.92E+06	8.99E+06	9.83E+02 ± 2.79E+01	1.69E+02	< 1.27E+02	5.38E-03	— ± —
J04151038+142354	04 15 10.339	+14 23 54.538	0.66	48.01	9.69E+06	8.00E+06	8.38E+02 ± 4.48E+01	1.26E+02	< 1.05E+02	3.55E-03	— ± —
J04510241+1458167	04 51 02.409	+14 58 16.5s	0.67	40.79	8.04E+06	8.48E+06	9.70E+02 ± 8.07E+01	1.45E+02	1.99E+02 ± 4.93E+01	4.38E-03	8.34E-12 ± 1.85E-12
J04471851+0627113	04 47 18.508	+06 27 11.592	0.65	40.59	9.10E+06	7.53E+06	6.07B+02 ± 1.06E+02	1.10E+02	— ± —	—	— ± —
J05110971+1548574	05 11 09.688	+15 48 57.492	0.79	57.00	1.33E+07	1.65E+07	1.43E+03 ± 1.56E+02	1.47E+03	< 2.29E+02	6.62E-02	1.70E-11 ± 4.15E-12
J045223385+1043099	04 52 23.860	+10 43 09.912	0.65	52.12	6.07E+06	7.53E+06	6.80E+02 ± 1.41E+02	1.10E+02	— ± —	—	— ± —
J04412780+1404340	04 41 27.808	+14 04 34.104	0.60	49.21	5.70E+06	5.49E+06	1.18E+03 ± 4.06E+01	5.55E+01	4.90E+02 ± 9.06E+01	1.08E-03	3.08E-11 ± 3.98E-12
J02185464+3513053	02 18 54.633	+35 13 05.632	0.64	43.60	7.67E+06	7.09E+06	4.40E+02 ± 2.23E+01	9.59E+01	< 9.06E+01	2.45E-03	— ± —
J02263361+1522245	02 26 33.645	+15 22 24.483	0.88	57.09	3.07E+07	2.63E+07	6.00E+04 ± 8.90E+02	1.17E+04	< 1.73E+02	7.47E-01	1.72E-11 ± 6.57E-12
J022523774+1035655	02 52 37.762	-09 13 56.381	0.72	33.97	7.79B+06	1.13E+07	4.14B+02 ± 1.13E+01	3.23E+02	2.08E+01 ± 5.53E+00	1.22E-02	— ± —
J0300280+0744590	03 00 02.811	+07 44 59.102	0.88	23.79	2.67E+07	2.63E+07	1.77E+04 ± 2.19E+02	1.17E+04	< 1.12E+01	7.47E-01	2.93E-12 ± 7.19E-13
J0318510+0914426	03 18 15.099	+09 14 42.338	0.68	61.51	1.08E+07	8.99E+06	— ± —	—	< 1.31E+02	5.38E-03	— ± —
J03183830+3239570	03 18 38.323	+32 39 56.859	0.67	51.71	5.39E+06	8.48E+06	1.64E+02 ± 2.24E+01	1.45E+02	< 3.41E+01	4.38E-03	— ± —
J03202921+0827161	03 20 29.195	+08 27 16.003	0.78	31.77	1.54E+07	1.56E+07	3.18E+03 ± 8.83E+01	1.17E+03	1.75E+02 ± 3.32E+01	4.93E-02	— ± —
J03222810+2709219	03 22 28.139	+27 09 21.795	0.65	31.75	8.06E+06	7.53E+06	5.92E+02 ± 5.19E+02	1.10E+02	< 5.27E+01	2.95E-03	— ± —
J03330528+0457291	03 33 05.392	+04 57 29.216	0.69	54.99	8.83E+06	9.52E+06	8.34E+02 ± 1.24E+02	1.97E+02	< 1.68E+02	6.63E-03	— ± —
J03481189+0708464	03 48 11.892	+07 08 46.466	0.69	36.53	1.04E+07	9.52E+06	7.67E+02 ± 5.63E+01	1.97E+02	< 9.64E+01	6.63E-03	— ± —
J03524101+25484159	03 52 41.011	+25 48 15.995	0.72	44.46	1.04E+07	1.13E+07	1.23B+03 ± 1.44E+02	3.23E+02	— ± —	—	— ± —
J03590972+28228340	03 59 09.735	+26 28 33.953	0.70	35.86	6.68E+06	1.01E+07	3.84E+02 ± 4.77E+01	2.31E+02	< 8.98E+01	8.15E-03	— ± —
J04084015+2333257	04 08 40.176	+23 33 25.620	0.61	46.08	5.99E+06	5.85E+06	2.36E+02 ± 4.61E+01	6.42E+01	< 8.85E+01	1.37E-03	— ± —
J04092011+0807436	04 09 20.127	+08 07 43.707	0.81	199.84	1.63E+07	9.04B+07	9.04E+03 ± 1.01E+03	3.23E+03	< 3.16E+03	1.20E-01	— ± —
J04150713-1132156	04 15 07.150	-11 32 15.523	0.70	43.82	8.41E+06	1.01E+07	1.44B+03 ± 6.14E+01	2.31E+02	< 3.08E+01	8.15E-03	— ± —
J04161310+1853042	04 16 13.122	+18 53 04.202	0.63	45.61	7.87E+06	6.66E+06	5.65E+02 ± 2.89E+01	8.42E+01	< 9.84E+01	2.04E-03	— ± —
J04174767+1339422	04 17 47.693	+13 39 42.392	0.62	47.45	6.21E+06	6.24E+06	2.84E+02 ± 2.53E+01	7.38E+01	< 1.33E+02	1.69E-03	— ± —
J04184702+1521585	04 18 47.037	+13 21 58.732	0.64	46.14	7.62B+06	7.09E+06	4.65E+02 ± 2.72E+01	9.59E+01	< 9.96E+01	2.48E-03	— ± —
J04201057-1445400	04 20 10.585	-14 45 39.852	0.74	29.32	1.26E+07	1.26E+07	1.82E+03 ± 8.21E+01	4.78E+02	< 5.72E+01	1.89E-02	— ± —
J04210411+0316074	04 21 04.11s	+03 16 07.364	0.83	37.08	1.90E+07	2.04E+07	6.87E+03 ± 4.45E+01	3.67E+03	< 1.80E+02 ± 6.50E+01	2.09E-01	— ± —
J04223004+1026046	04 22 30.036	+10 26 04.602	0.60	47.89	5.74B+06	5.49E+06	1.77E+02 ± 6.57E+01	5.55E+01	< 2.06E+02	1.08E-03	— ± —
J04240740+2207079	04 24 07.426	+22 07 07.930	0.72	45.78	1.18E+07	1.13E+07	1.21E+03 ± 1.96E+02	3.23E+02	— ± —	—	— ± —
J04252002+2306312	04 25 20.039	+23 06 31.115	0.60	53.48	5.84E+06	5.49E+06	2.57E+02 ± 8.72E+01	5.55E+01	< 9.67E+01	1.08E-03	— ± —
J04264760+2114059	04 26 47.618	+21 14 05.716	0.67	43.20	9.63E+06	9.43E+06	9.93E+02 ± 1.25E+02	1.45E+02	— ± —	—	— ± —
J04274170+4655395	04 27 41.719	+46 55 39.466	0.81	68.77	5.25E+07	8.83E+07	2.31E+04 ± 8.16E+02	3.23E+03	< 2.49E+02	1.20E-01	— ± —
J04293897+2252379	04 29 38.994	+22 52 57.812	0.74	59.35	1.29B+07	1.26E+07	1.99E+03 ± 1.63E+02	4.78E+02	< 2.60E+02	1.88E-02	2.36E-11 ± 4.35E-12
J04303819+2254289	04 30 38.194	+22 54 28.882	0.66	50.93	8.27E+06	8.00E+06	1.77E+03 ± 1.58E+02	1.26E+02	3.81E+02 ± 1.18E+02	3.58E-03	— ± —
J04324094+1906484	04 32 40.945	+19 06 48.534	0.78	52.53	1.64E+07	1.56E+07	4.51E+03 ± 2.56E+02	1.17E+03	— ± —	—	— ± —
J04333890+4951407	04 33 18.903	+49 51 40.705	0.80	46.37	1.08E+07	1.74E+07	1.36E+03 ± 8.84E+01	1.85E+03	< 1.72E+02	8.94E-02	— ± —
J04343992+1512325	04 34 39.936	+15 12 32.589	0.65	48.07	8.90B+06	7.53E+06	— ± —	—	3.72E+02 ± 2.26E+01	2.41E-11 ± 3.79E-12	— ± —
J04352355+0839304	04 35 02.550	+08 39 30.564	0.79	59.34	1.65E+07	1.65E+07	2.73E+03 ± 6.78E+01	1.47E+03	5.19E+02 ± 1.57E+02	6.62E-02	3.34E-11 ± 4.88E-12
J04373823+0440111	04 37 38.241	+04 40 11.199	0.70	48.32	9.70E+06	1.01E+07	6.91E+02 ± 9.75E+01	2.31E+02	< 2.15E+02	8.15E-03	— ± —
J04402429+0213522	04 40 42.484	+02 13 52.012	0.64	23.91	6.34E+06	7.09E+06	1.85E+02 ± 6.44E+00	9.59E+01	< 2.56E+01	2.48E-03	— ± —
J0443267+1518538	04 43 12.673	+15 18 53.753	0.60	52.52	3.50E+06	5.49E+06	3.06E+02 ± 5.97E+01	5.55E+01	< 2.56E+02	1.08E-03	— ± —
J04451961+1334374	04 45 19.614	+13 34 27.437	0.66	51.71	7.64E+06	8.00E+06	2.33E+03 ± 1.45E+02	1.26E+02	4.74E+02 ± 8.56E+01	3.55E-03	2.32E-11 ± 3.35E-12
J04470612+1543419	04 47 06.481	+15 43 41.787	0.90	60.34	2.40B+07	2.91E+07	3.29E+04 ± 1.30E+02	1.91E+04	< 1.23E+02	1.40E+00	— ± —
J04470892+2052564	04 47 08.933	+20 52 56.336	0.82	42.30	1.86E+07	1.93E+07	6.81E+03 ± 1.14E+02	2.91E+03	< 8.98E+01	1.60E-01	— ± —
J04470974+2401124	04 47 09.753	+24 01 12.131	0.61	46.15	6.58E+06	5.85E+06	3.45E+02 ± 8.88E+01	6.42E+01	— ± —	—	— ± —
J04473532+1453209	04 47 35.335	+14 53 20.725	0.67	47.84	9.95E+06	8.48E+06	8.74E+02 ± 2.27E+01	1.45E+02	< 1.53E+02	4.38E-03	— ± —
J04513356+1417109	04 51 33.578	+14 17 10.942	0.88	75.82	2.39E+07	2.63E+07	5.88E+03 ± 3.47E+02	1.17E+04	< 2.64E+02	7.47E-01	— ± —
J04514917+1716255	04 51 49.187	+17 16 16.2394	0.73	54.47	1.17E+07	1.19E+07	1.41E+03 ± 5.10E+01	3.90E+02	< 2.20E+02	1.55E-02	— ± —

Table 4 continued

Table 4 (continued)

Name ^a	RA	Dec	Mass	Dist.	F_J	σ_J	F_{NUV}	σ_{NUV}	F_{FUV}	σ_{FUV}	f_X
	2MASS	2MASS	[M_\odot]	[pc]	[μJy]	[μJy]	[μJy]	[μJy]	[μJy]	[μJy]	[erg cm $^{-2}$ s $^{-1}$]
J04524755+2238503	04 52 47.561	+22 38 50.132	0.70	55.94	1.17E+07	1.01E+07	1.58E+03 ± 1.00E+02	< 1.96E+02	2.31E+02	8.15E-03	— ± —
JO45413192-1154506	04 54 31.939	-11 54 50.515	0.81	35.49	1.82E+07	1.83E+07	5.88E+03 ± 1.70E+02	2.32E+03	6.44E+01 ± 4.195E+01	1.20E-01	5.01E-12 ± 1.60E-12
JO4594939+1958003	04 59 49.508	+19 58 00.356	0.89	149.16	1.70E+08	2.77E+07	3.70E+05 ± 4.20E+03	1.49E+04	< 1.57E+03	1.02E+00	— ± —
J05004888+0443591	05 00 48.886	+04 43 59.21s	0.85	52.06	2.46E+07	2.26E+07	1.86E+04 ± 1.25E+02	5.80E+03	4.23E+02 ± 1.46E+02	3.45E-01	— ± —
J05012217+2955475	05 01 22.170	+29 55 47.596	0.90	90.51	5.34E+07	2.91E+07	3.90E+04 ± 8.34E+02	1.91E+04	< 5.24E+02	1.40E+00	— ± —
J05013765+1224589	05 01 37.665	+12 24 58.99	0.80	51.46	1.37E+07	1.74E+07	1.05E+03 ± 1.29E+02	1.85E+03	< 1.94E+02	8.94E-02	— ± —
J05030708+1901048	05 03 07.101	+19 01 04.779	0.62	53.34	9.26E+06	6.24E+06	7.51E+02 ± 3.58E+01	7.38E+01	< 1.73E+02	1.63E-03	— ± —
J05054038+0627545	05 05 40.377	+06 27 54.632	0.87	56.51	3.84E+07	2.51E+07	2.56E+04 ± 4.04E+02	9.19E+03	< 3.59E+02	5.60E-01	— ± —
J05072527+1841339	05 07 35.292	+18 41 33.807	0.75	68.78	1.47E+07	1.33E+07	2.89E+03 ± 4.25E+02	5.92E+02	< 2.61E+02	2.35E-02	— ± —
J05081333+2159250	05 08 13.336	+21 59 24.884	0.64	62.76	6.83E+06	7.09E+06	4.97E+02 ± 1.43E+02	9.59E+01	— ± —	—	— ± —
J05102443+1025047	05 10 24.438	+10 25 04.795	0.68	67.80	1.17E+07	8.99E+06	1.33E+03 ± 1.89E+02	1.69E+02	— ± —	—	— ± —
J05115547+0542578	05 11 55.474	+05 42 57.863	0.89	69.88	2.30E+07	2.77E+07	1.48E+04 ± 2.17E+02	1.49E+04	< 4.92E+02	1.02E+00	— ± —
J05122408+1824086	05 12 24.082	+18 24 08.641	0.61	53.09	7.32E+06	5.85E+06	5.21E+02 ± 1.15E+02	6.42E+01	< 2.10E+02	1.37E-03	— ± —
J05505408+0609242	05 50 54.091	+06 09 24.194	0.81	355.34	5.68E+08	1.83E+07	2.09E+05 ± 1.32E+04	2.32E+03	< 1.71E+04	1.20E-01	— ± —
Field, 5 Gyr											
HD 55	00 05 17.6886	-67 49 57.322	0.70	16.39	1.14E+07	1.07E+07	2.01E+03 ± 1.79E+01	2.61E+02	< 1.79E+01	9.10E-03	— ± —
GJ 3.008	00 08 27.2796	+17 25 27.459	0.61	21.74	5.68E+06	6.13E+06	3.24E+02 ± 1.65E+01	6.79E+01	4.07E+01 ± 1.11E+01	1.38E-03	— ± —
HD 870	00 12 50.2493	-57 54.45.395	0.89	20.63	3.10E+07	3.24E+07	> 5.12E+04	3.07E+04	1.62E+02 ± 1.97E+01	2.52E+00	— ± —
CD-46 76	00 21 19.6196	-45 44 47.109	0.61	17.59	5.35E+06	6.13E+06	1.83E+02 ± 1.17E+01	6.79E+01	8.94E+00 ± 4.00E+00	1.38E-03	— ± —
HD 2025	00 24 23.9333	-27 01 36.380	0.79	17.95	1.71E+07	1.82E+07	8.91E+03 ± 5.46E+01	2.23E+03	5.54E+01 ± 8.15E+00	1.22E-01	— ± —
54 Psc	00 39 21.80589	+21 15 01.7081	0.86	11.14	3.22E+07	2.71E+07	> 1.69E+04	1.34E+04	5.99E+01 ± 7.16E+00	9.74E-01	— ± —
HD 3765	00 40 49.26909	+40 11 13.8306	0.83	17.94	2.71E+07	1.77E+07	1.03E+04 ± 2.54E+01	5.21E+03	3.12E+01 ± 1.14E+00	4.45E-01	1.17E-12 ± 3.60E-13
CD-34 239	00 41 30.47339	-33 37 32.932	0.57	19.63	5.07E+06	4.78E+06	1.45E+02 ± 1.09E+01	3.70E+01	< 1.80E+01	5.14E-04	— ± —
HD 4256	00 45 04.8939	+01 47 07.878	0.79	22.43	2.41E+07	1.82E+07	8.47E+03 ± 1.85E+01	2.23E+03	3.80E+01 ± 2.32E+00	1.22E-01	— ± —
HD 4628	00 48 22.97665	+05 16 50.2129	0.79	7.43	1.57E+07	1.82E+07	— ± —	—	2.40E+01 ± 2.62E+00	1.22E-01	— ± —
CD-50 210	00 49 01.7119	-50 08 41.708	0.61	23.10	6.43E+06	6.13E+06	2.28E+02 ± 1.76E+01	6.79E+01	3.79E+01 ± 1.16E+01	1.38E-03	— ± —
HD 4913	00 51 21.7540	+18 44 21.293	0.65	22.24	1.31E+07	7.91E+06	1.17E+03 ± 4.19E+01	1.24E+02	2.68E+01 ± 1.02E+01	5.17E-03	8.45E-13 ± 3.07E-13
HD 4967	00 51 34.0200	-22 54 36.241	0.70	15.34	9.04E+06	1.07E+06	1.07E+02 ± 2.54E+01	2.61E+01	1.81E+01 ± 7.24E+00	9.10E-03	— ± —
HD 6101	01 02 24.57273	+05 03 41.2140	0.83	15.21	1.22E+07	2.27E+07	3.81E+03 ± 7.34E+00	5.21E+03	4.04E+01 ± 1.16E+00	2.45E-01	— ± —
BD+79 38	01 21 36.9120	+80 09 06.480	0.70	24.42	1.12E+07	1.07E+07	9.96E-02 ± 5.06E+01	2.61E+02	— ± —	—	— ± —
HD 7924	01 21 53.1136	+76 42 37.039	0.89	17.00	3.12E+07	3.24E+07	> 2.74E+04	3.07E+04	6.95E+01 ± 9.16E+00	9.74E-01	3.70E-13 ± 1.30E-13
HD 9540	01 33 15.8091	-24 10 40.654	0.89	19.27	3.12E+07	3.24E+07	— ± —	—	2.06E+02 ± 2.13E+01	2.52E+00	8.43E-13 ± 2.21E-13
HD 9770	01 35 01 03508	-29 54 37.0162	0.83	26.02	4.42E+07	1.71E+07	> 2.08E+05	1.92E+02	2.77E+03 ± 1.29E+02	9.74E-01	1.51E-10 ± 4.03E-12
GJ 68	01 42 29.76174	+12 24 42.385	0.74	7.61	1.56E+07	1.36E+07	> 1.66E+05	5.87E+02	4.97E+01 ± 9.51E-01	1.82E+00	— ± —
HD 10953	01 46 38.5410	-21 11 47.232	0.61	23.75	1.08E+07	6.13E+07	4.36E+03 ± 6.55E+01	5.87E+01	6.83E+01 ± 2.17E+01	1.88E-02	— ± —
BD-21 397	02 13 12.1645	+56 33 35.72	0.86	31.93	3.74E+07	2.71E+07	1.51E+04 ± 2.20E+02	1.92E+01	7.55E+01 ± 1.625E+01	1.38E-03	1.11E-12 ± 4.77E-13
HD 14039	02 18 24.602	+53 23 21.6702	0.70	14.76	6.48E+06	6.37E+06	> 2.53E+05	3.26E+01	2.24E+01 ± 2.64E+00	1.22E-01	1.73E-13 ± 4.86E-14
GJ 105 A	02 36 04.89466	+06 53 12.7466	0.60	7.24	1.14E+07	6.13E+06	8.60E+02 ± 4.87E+01	2.61E+02	— ± —	—	— ± —
BD+00 444	02 40 42.8731	+01 11 55.240	0.61	23.94	8.54E+06	10.07E+07	7.16E+02 ± 4.63E+01	2.61E+02	— ± —	—	— ± —
BD+02 418	02 42 33.5410	+03 22 22.063	0.70	24.61	7.27E+07	7.91E+06	1.09E+03 ± 2.66E+01	1.24E+02	1.83E+01 ± 5.38E+00	5.17E-03	— ± —
HD 17230	02 46 17.2768	+11 46 30.855	0.65	16.15	2.26E+07	2.26E+07	4.81E+02 ± 2.35E+01	2.61E+02	3.67E+01 ± 1.09E+01	9.10E-03	— ± —
CD-23 1056	02 46 42.8871	-23 05 11.803	0.70	23.39	8.26E+06	1.07E+07	2.23E+02 ± 3.35E+00	2.61E+02	< 8.76E+00	9.10E-03	— ± —
BD+33 529	02 52 07.13773	+34 23 21.6702	0.70	14.76	5.24E+06	1.07E+07	1.07E+03 ± 1.85E+01	2.61E+02	2.93E+01 ± 9.49E+00	9.10E-03	— ± —
BD+19 451	03 03 49.0599	+20 06 39.126	0.70	21.37	1.65E+07	1.07E+07	3.12E+03 ± 5.88E+01	6.79E+01	— ± —	—	— ± —
BD-02 418	02 42 33.5410	+08 58 50.56	0.71	23.13	1.08E+07	1.07E+07	> 1.64E+05	2.71E+02	8.00E+01 ± 2.36E+01	9.74E-01	— ± —
HD 20165	03 14 47.2268	-49 58 30.914	0.74	19.30	1.38E+07	1.36E+07	3.07E+03 ± 1.85E+01	5.87E+02	2.17E+01 ± 3.49E+00	1.88E-02	2.00E-13 ± 8.63E-14
HD 21209	03 23 17.1764	-40 04 53.027	0.74	17.70	1.75E+07	1.36E+07	> 2.04E+04	5.87E+02	2.04E+03 ± 4.84E+01	2.52E+00	1.02E-11 ± 8.11E-13

Table 4 continued

Table 4 (continued)

Name ^a	RA	Dec	Mass	Dist.	F_J	σ_J	F_{NUV}	σ_{NUV}	F_{FUV}	σ_{FUV}	f_X
	2MASS	2MASS	[M_\odot]	[pc]	[μJy]	[μJy]	[μJy]	[μJy]	[μJy]	[μJy]	[erg cm $^{-2}$ s $^{-1}$]
HD 21197	03 24 59.7306	-05 21 49.518	0.74	15.35	1.75E+07	1.36E+07	2.72E+03 \pm 9.85E+00	5.87E+02	5.21E+01 \pm 2.84E+00	1.88E-02	7.17E-13 \pm 2.13E-13
HD 21749	03 26 53.2226	-63 29 56.763	0.70	16.33	1.57E+07	1.07E+07	3.03E+03 \pm 6.32E+01	2.61E+03	< 7.92E+00	9.10E-03	— ± —
GJ 144	03 32 55.84496	-07 27 29.7312	0.86	3.20	2.00E+07	2.60E+07	> 1.92E+06	1.42E+02 \pm 3.05E+00	2.45E-01	2.29E-12 \pm 6.33E-14	
BD-16 502	03 43 52.56442	+16 40 19.305	0.65	17.21	7.17E+06	7.91E+06	3.30E+02 \pm 1.22E+01	1.24E+02	2.23E+01 \pm 5.61B+00	5.17E-03	— ± —
HD 23356	03 43 53.3429	-19 06 39.232	0.62	13.96	1.04E+07	6.24E+06	> 7.37E+04	7.38E+01	3.39E+01 \pm 5.98E+00	2.45E-01	1.15E-12 \pm 2.02E-13
HD 23484	03 44 09.1730	-38 16 54.371	0.86	16.17	2.81E+07	2.38E+07	> 2.22E+05	7.28E+03	1.52E+02 \pm 2.27E+01	2.45E-01	1.49E-12 \pm 3.66E-13
HD 24238	03 55 03.8426	+61 10 00.505	0.83	21.01	2.54E+07	1.53E+07	> 1.06E+05	1.29E+02	< 2.98E+01	2.45E-01	— ± —
HD 24451	04 01 19.62185	+76 09 33.7332	0.74	16.23	1.46E+07	2.90E+03 \pm 4.87E+01	5.87E+02	8.41E+01 \pm 1.28E+01	8.48E-02	2.97E-13 \pm 8.88E-14	
HD 25665	04 09 35.0401	+69 32 29.011	0.79	18.77	1.82E+07	1.14E+04 \pm 1.89E+01	2.23E+03	4.40E+01 \pm 2.46E+00	1.22E-01	— ± —	
BD-04 782	04 15 09.52878	-04 25 05.9763	0.70	35.09	2.91E+07	1.07E+07	3.26E+03 \pm 1.20E+02	2.61E+02	< 7.59E+01	9.10E-03	— ± —
GJ 166 A	04 15 16.31963	-07 39 10.3404	0.89	5.04	4.30E+07	3.21E+07	> 5.90E+05	3.11E+04	< 2.55E+00	2.52E+00	— ± —
HD 26900	04 16 32.65550	+36 30 06.574	0.83	24.53	2.28E+07	2.27E+07	1.49E+04 \pm 4.85E+01	5.21E+03	1.14E+02 \pm 3.40E+01	2.45E-01	2.26E-12 \pm 5.29E-13
CD-20 550	04 21 31.6088	-19 45 23.345	0.70	24.61	6.71E+06	1.07E+07	3.86E+02 \pm 2.61E+01	2.61E+02	< 1.96E+01	9.10E-03	— ± —
HD 29883	04 43 35.43558	+27 41 14.648	0.70	21.86	1.27E+07	1.07E+04 \pm 5.04E+01	2.61E+02	— ± —	—	—	—
LHS 199	04 55 57.594	-61 09 45.91	0.61	24.00	2.22E+06	6.13E+06	4.50E+02 \pm 2.78E+00	6.79E+01	< 2.03E+01	1.38E-03	— ± —
HD 32450	05 02 28.42030	-21 15 23.9203	0.61	8.38	7.39E+06	6.13E+06	2.74B+02 \pm 4.22E+00	6.79E+01	5.44E+00 \pm 1.10E+00	1.33E-03	1.83E-13 \pm 5.78E-14
CD-23 2363	05 03 21.88545	-23 15 00.8542	0.65	23.20	1.79E+07	7.91E+06	1.12E+03 \pm 2.88E+01	1.24E+02	3.88E+01 \pm 1.05E+01	5.11E-03	— ± —
L 233-30	05 17 53.48	-53 40 52.5	0.79	89.12	5.18E+06	1.82E+07	— ± —	—	< 2.92E+02	1.22E-01	— ± —
CD-42 1943	05 26 34.0189	-42 20 15.514	0.83	19.88	4.93E+06	1.27E+07	1.41B+02 \pm 1.77E+01	5.21B+03	< 2.21E+01	2.45E-01	— ± —
HD 36003	05 28 26.0955	-03 29 58.400	0.70	12.94	1.51E+07	1.07E+07	1.82E+03 \pm 4.16E+01	2.61E+02	— ± —	—	—
HD 37008	05 38 11.86172	+51 26 44.6719	0.86	20.51	2.37E+07	2.71E+07	— ± —	—	2.86E+01 \pm 9.74E+00	9.74E-01	— ± —
BD+42 780	05 45 48.2757	+62 14 12.386	0.61	13.51	8.37E+06	6.13E+06	7.19E+02 \pm 2.26E+01	6.79E+01	2.08E+01 \pm 3.73E+00	1.33E-03	— ± —
CD-48 1982	05 47 18.2143	-48 31 30.504	0.61	20.79	1.01E+07	6.13E+06	7.19E+02 \pm 2.26E+01	6.79E+01	2.45E+01 \pm 9.67E+00	1.33E-03	1.23E-12 \pm 2.23E-13
HD 40307	05 54 04.233991	-60 01 24.4977	0.79	12.94	1.83E+07	1.82E+07	— ± —	—	1.24E+01 \pm 3.95E+00	1.22E-01	— ± —
LHS 1865	06 44 45.693310	+71 53 15.4480	0.61	21.53	3.37E+06	6.13E+06	1.74B+02 \pm 1.44E+01	6.79E+01	< 3.09E+01	5.09E-13	± 2.02E-13
HD 48948	06 49 57.02556	+60 20 07.361	0.70	16.91	1.33E+07	1.07E+07	1.31B+03 \pm 7.38E+00	2.61E+02	2.08E+01 \pm 7.74E+00	9.74E-01	— ± —
BD+40 1758	06 56 28.11811	+40 04 27.5872	0.70	25.15	1.56E+07	1.07E+07	— ± —	—	2.08E+01 \pm 3.73E+00	1.33E-03	— ± —
HD 266611	06 57 04.68907	+30 45 23.3758	0.70	18.89	8.24B+06	1.07E+07	5.37E+02 \pm 1.62E+01	2.61E+02	2.43E+01 \pm 1.10E+01	9.10E-03	— ± —
MCC 484	07 01 06.1884	+59 49 59.830	0.70	22.14	4.38E+06	1.07E+07	1.90E+02 \pm 1.63E+01	2.61E+02	< 2.81E+01	9.10E-03	— ± —
HD 53680	07 03 50 23558	-43 33 40.8161	0.65	17.30	1.25E+07	7.91E+06	1.10E+03 \pm 4.40E+01	1.24E+02	— ± —	—	—
HD 53927	07 08 04.2389	+29 50 04.185	0.79	23.01	1.86E+07	1.07E+07	1.20B+04 \pm 7.76E+01	2.23E+03	5.43E+01 \pm 9.34E+00	1.22E-01	— ± —
BD-14 1750	07 10 49.5790	-14 25 38.925	0.70	23.36	8.84E+06	1.07E+07	6.00E+02 \pm 4.25E+01	2.61E+02	— ± —	—	—
HD 59582	07 31 07.7116	+14 36 50.915	0.70	20.75	1.27E+07	1.07E+07	1.80E+03 \pm 3.98E+01	2.61E+02	< 1.21E+01	9.10E-03	— ± —
HD 63991	07 52 47.4276	+25 55 35.344	0.74	21.88	1.65E+07	1.36E+07	4.09E+03 \pm 2.19E+01	5.87E+02	3.95E+01 \pm 4.19E+00	1.88E-02	— ± —
HD 68834	08 14 35.9143	+13 01 22.174	0.70	19.19	1.32E+07	1.07E+07	1.74E+03 \pm 1.22E+01	2.61E+02	2.72E+01 \pm 7.49E+00	9.10E-03	— ± —
BD+31 1781	08 18 10.7790	+30 36 02.944	0.70	22.86	1.62E+07	1.07E+07	2.37E+03 \pm 1.21E+01	2.61E+02	3.44E+01 \pm 2.97E+00	9.10E-03	— ± —
LHS 2018	08 29 55.3283	+61 32 32.738	0.61	20.31	5.96E+06	6.13E+06	2.76E+02 \pm 1.36E+01	6.79E+01	< 3.09E+01	1.33E-03	— ± —
HD 72760	08 34 31.6500	-00 43 33.864	0.92	21.10	5.26E+07	3.21E+07	> 3.46E+06	3.11E+04	3.06E+02 \pm 7.45E+00	4.03E+00	4.03E+00
HD 73697	08 39 50.7918	+11 31 21.618	0.83	18.46	2.19E+07	2.27E+07	< 1.25E+01	5.21E+03	1.43E+01 \pm 5.87E+00	2.45E-01	— ± —
HD 74377	08 45 10.3963	+41 40 18.604	0.79	24.97	2.09E+07	1.82E+07	7.22E+03 \pm 2.95E+01	2.23E+03	< 2.83E+01	1.22E-01	— ± —
HD 77175 A	09 01 17.478	+15 15 56.82	0.70	18.47	1.15E+07	1.07E+07	1.20E+03 \pm 3.34E+00	2.61E+02	1.94E+01 \pm 3.34E+00	9.10E-03	— ± —
HD 79210	09 14 22.79157	+52 41 11.7206	0.61	6.33	7.08E+06	6.13E+06	4.14E+02 \pm 6.06E+00	6.79E+01	2.23E+01 \pm 3.51E+00	1.33E-03	5.55E-13 \pm 6.09E-14
GJ 338 B	09 14 24.6778	+52 41 10.919	0.61	6.33	7.83E+06	6.13E+06	4.02E+02 \pm 5.97E+00	6.79E+01	2.24E+01 \pm 3.49E+00	1.33E-03	5.54E-13 \pm 6.09E-14
HD 79555	09 14 53.65814	+04 26 34.4517	0.74	17.80	1.36E+07	7.61E+03 \pm 2.73E+01	5.87E+02	1.73E+02 \pm 5.90E+00	1.88E-02	9.44E-12 \pm 7.59E-13	
BD+27 1739	09 18 21.5230	+27 18 41.626	0.70	20.98	1.09E+07	1.07E+07	8.97E+02 \pm 9.50E+00	2.61E+02	6.19E+01 \pm 9.82E+00	9.10E-03	1.30E-12 \pm 4.37E-13
HD 80632	09 20 44.3171	-05 45 14.302	0.74	24.18	1.52E+07	1.36E+07	1.92E+03 \pm 5.56E+01	5.87E+02	4.44E+01 \pm 1.45E+01	1.88E-02	— ± —
HD 80768	09 26 53.1297	+75 56 03.340	0.61	20.95	1.30E+07	6.13E+06	1.77E+03 \pm 5.55E+01	6.79E+01	6.86E+01 \pm 2.04E+01	1.33E-03	7.52E-13 \pm 1.69E-13
BD+1-81 297	09 27 56.1794	+80 34 48.811	0.61	23.10	1.32E+07	6.13E+06	1.14E+03 \pm 1.28E+01	6.79E+01	2.17E+01 \pm 9.41E+00	1.33E-03	— ± —

Table 4 continued

THE UV AND X-RAY EVOLUTION OF K STARS

Table 4 (continued)

Name ^a	RA	Dec	Mass	Dist.	F_J	σ_J	F_{NUV}	σ_{NUV}	F_{FUV}	σ_{FUV}	f_X
	2MASS	2MASS	[M_\odot]	[pc]	[μJy]	[μJy]	[μJy]	[μJy]	[μJy]	[μJy]	[erg cm $^{-2}$ s $^{-1}$]
BD-04 2639	09 29 35.05287	-05 22 21.7364	0.61	24.18	1.03E+07	6.13E+06	8.02E+02 \pm 3.80E+01	6.79E+01	6.51E+01 \pm 2.05E+01	1.38E-03	- \pm -
HD 82106	09 29 54.8252	+05 39 18.472	0.79	12.78	1.75E+07	1.82E+07	-	-	1.00E+02 \pm 3.41E+00	1.21E-01	2.03E-12 \pm 2.43E-13
BD+23 2121	09 37 11.3404	+22 41 38.910	0.70	22.55	1.25E+07	1.07E+07	9.82E+02 \pm 2.17E+01	2.61E+02	2.15E+01 \pm 5.59E+00	9.10E-03	- \pm -
HD 84035	09 43 25.66143	+42 41 29.6141	0.74	18.03	1.89E+07	1.36E+07	2.79E+03 \pm 1.58E+01	5.87E+02	1.70E+01 \pm 7.67E+00	1.88E-02	1.44E-12 \pm 3.23E-13
HD 85488	09 52 11.36258	+03 13 18.6347	0.70	20.54	1.41E+07	1.07E+07	1.59E+03 \pm 1.44E+01	2.61E+02	< 1.89E+01	9.10E-03	- \pm -
HD 87883	10 08 43.1400	+34 14 32.133	0.89	18.30	2.47E+07	3.24E+07	1.08E+04 \pm 2.19E+01	3.07E+04	7.21E+01 \pm 1.67E+01	2.52E+00	- \pm -
BD-75 403	10 10 58.1301	+75 08 28.9261	0.65	21.07	1.24E+07	7.91E+06	7.33E+02 \pm 3.82E+01	1.24E+02	< 3.14E+01	5.17E-03	- \pm -
GJ 380	10 11 22.14051	+49 27 15.2567	0.61	42.87	9.76E+06	6.42E+02 \pm 5.11E+00	6.79E+01	2.89E+01 \pm 2.36E+00	2.84E-13	- \pm -	
HD 233719	10 13 57.38220	+52 30 24.2141	0.65	22.97	9.53E+06	7.91E+06	1.21E+03 \pm 1.33E+01	1.24E+02	< 2.44E+01	5.17E-03	- \pm -
36 UMa B	10 30 23.3093	+55 59 56.850	0.61	12.92	9.49E+06	6.13E+06	< 5.21E+00	6.79E+01	3.25E+01 \pm 7.96E+00	1.38E-03	- \pm -
BD+46 1635	10 31 24.2177	+45 31 33.779	0.61	16.01	1.18E+07	6.13E+06	8.25E+02 \pm 1.93E+01	6.79E+01	1.79E+01 \pm 6.79E+00	1.18E-12 \pm 2.56E-13	- \pm -
BD+57 1274	10 31 43.2242	+57 06 57.107	0.70	17.56	7.93E+06	1.07E+07	5.25E+02 \pm 1.08E+00	2.61E+02	2.14E+01 \pm 5.83E+01	9.10E-03	8.71E-13 \pm 2.04E-13
BD-76 404	10 54 25.5092	+76 03 56.709	0.65	23.01	1.00B+07	7.91E+06	1.12B+03 \pm 4.92E+01	1.24E+02	< 2.56E+01	5.17E-03	- \pm -
BD-18 3106	11 07 27.70340	-19 17 29.3321	0.70	18.73	5.86E+06	1.07E+07	3.97E+02 \pm 1.99E+01	2.61E+02	8.93E+01 \pm 1.69E+01	9.10E-03	- \pm -
HD 96612	11 08 14.0146	+38 25 35.874	0.89	22.82	1.96E+07	3.24E+07	9.84E+03 \pm 1.12E+02	3.07E+04	< 1.51E+01	2.52E+00	- \pm -
HD 97101	11 11 05.1720	+30 26 45.663	0.61	11.89	1.12B+07	6.13E+06	6.67B+02 \pm 1.60E+01	6.79E+01	2.25E+01 \pm 5.09E+00	1.38E-03	- \pm -
HD 97214	11 11 10.7008	-10 57 03.192	0.70	19.87	9.04E+06	1.07E+07	1.17E+03 \pm 3.29E+01	2.61E+02	< 2.37E+01	9.10E-03	- \pm -
HD 97503	11 13 13.2345	+04 28 56.437	0.70	18.36	1.29E+07	1.07E+07	2.14E+03 \pm 1.23E+01	2.61E+02	4.34E+01 \pm 1.27E+01	9.10E-03	5.40E-13 \pm 1.29E-13
HD 97658	11 14 33.1613	+25 42 37.390	0.61	21.58	7.49E+06	6.13E+06	> 1.73E+04	6.79E+01	4.08E+01 \pm 1.15E+01	9.74E-01	- \pm -
HD 97782	11 14 48.17139	-23 06 17.7241	0.70	23.11	1.66E+07	1.07E+07	1.61E+03 \pm 6.01E+01	2.61E+02	< 2.67E+01	9.10E-03	- \pm -
BD-13 3333	11 16 22.1464	-14 41 36.155	0.61	18.27	6.51E+06	6.13E+06	3.63B+02 \pm 1.04E+01	6.79E+01	3.48E+01 \pm 1.02E+01	1.38E-03	- \pm -
CD-27 7978	11 17 07.5069	-27 48 48.715	0.61	17.67	7.49E+06	6.13E+06	4.55E+02 \pm 2.35E+01	6.79E+01	4.46E+01 \pm 1.37E+01	9.10E-03	- \pm -
GJ 3662	11 24 53.7800	+40 00 12.675	0.74	23.47	8.45E+06	1.36E+07	4.92E+02 \pm 3.29E+01	5.87E+02	2.59E+01 \pm 1.18E+01	1.88E-02	- \pm -
BD+63 965	11 31 13.0920	+63 09 27.122	0.61	23.01	9.28E+06	6.13E+06	7.47E+02 \pm 7.20E+00	6.79E+01	8.44E+01 \pm 1.59E+01	1.25E-12 \pm 3.94E-13	- \pm -
BD+51 1697	11 47 03.4988	+50 58 18.500	0.74	23.57	1.20B+07	1.36E+07	1.23B+03 \pm 3.80E+01	5.87E+02	6.85E+01 \pm 2.08E+01	1.88E-02	1.40E-12 \pm 5.31E-13
HD 104067	11 59 10.0090	+20 21 13.612	0.83	20.58	2.17E+07	9.57E+03 \pm 1.36E+02	5.21E+03	-	-	-	- \pm -
HD 238090	12 12 20.8595	+54 29 08.724	0.70	15.24	6.59B+06	1.07E+07	3.31E+02 \pm 4.67E+00	2.61E+02	< 6.74B+00	9.10E-03	- \pm -
BD+49 2126	12 15 08.8430	+48 43 57.258	0.65	22.46	7.27E+06	7.91E+06	4.30B+02 \pm 2.39E+00	1.24E+02	3.08E+01 \pm 1.27E+00	5.17E-03	- \pm -
HD 107576	12 21 59.84698	-41 03 33.2576	0.74	24.44	2.00E+07	1.36E+07	4.69E+03 \pm 7.82E+01	5.87E+02	< 4.29E+01	1.88E-02	- \pm -
HD 107888	12 23 53.5526	+12 34 48.911	0.70	21.48	7.47E+06	1.07E+07	3.11E+02 \pm 3.60E+00	2.61E+02	1.01E+01 \pm 1.73B+00	9.10E-03	- \pm -
HD 110315	12 41 06.4777	+15 22 36.006	0.70	14.11	1.47E+07	1.07E+07	9.37E+03 \pm 1.36E+02	5.21E+03	5.21E+01 \pm 1.02E+01	1.38E-03	- \pm -
HD 110833	12 44 14.54514	+45 33.4882	0.74	15.00	1.51E+07	1.36E+07	> 2.35E+04	5.87E+02	8.05E+01 \pm 3.95E+00	9.10E-03	- \pm -
HD 112575	12 57 43.95596	-14 27 48.6288	0.70	25.64	1.50B+07	1.07E+07	2.62E+03 \pm 4.57E+01	2.61E+02	< 4.19E+01	9.10E-03	- \pm -
HD 113827	13 05 41.4079	+49 28 18.964	0.74	21.60	1.11B+07	1.36E+07	1.68E+03 \pm 3.88E+00	5.87E+02	4.16E+01 \pm 1.93E+00	1.88E-02	1.23E-12 \pm 3.43E-13
BD+21 2486	13 06 15.39818	+20 43 45.2749	0.74	19.71	1.15E+07	1.36E+07	3.11E+02 \pm 1.60E+00	2.61E+02	9.78E+01 \pm 1.95E+01	1.88E-02	3.90E-12 \pm 4.28E-13
BD+35 2406	13 07 35.0630	+34 24 06.061	0.79	24.80	1.38E+07	1.82E+07	1.89E+03 \pm 2.10E+01	2.23E+03	4.58E+01 \pm 1.14E+01	1.22E-01	- \pm -
HD 114783	13 12 43.78556	-02 15 54.1335	0.79	21.08	1.85E+07	1.07E+07	> 1.49E+04	5.66E+01 \pm 8.92E+00	9.10E-03	- \pm -	
HD 238224	13 23 23.29688	+57 54 22.1403	0.70	24.12	1.25E+07	1.07E+07	1.55E+03 \pm 4.70E+01	2.61E+02	1.36E+02 \pm 2.81E+01	5.15E-03	8.55E-12 \pm 7.48E-13
HD 116443	13 23 40.8451	+02 43 39.987	0.70	16.57	8.67E+06	1.07E+07	> 2.10E+04	2.61E+02	4.11E+01 \pm 1.14E+01	2.42E-01	5.61E-13 \pm 2.27E-13
HD 117936	13 33 32.4004	+08 35 12.345	0.79	18.05	1.85E+07	1.82E+07	5.45E+03 \pm 9.28E+01	2.23E+03	7.02E+01 \pm 1.65E+01	1.22E-01	1.45E-12 \pm 3.91E-13
HD 118096	13 34 03.2376	+33 13 42.211	0.74	22.68	1.10E+07	1.36E+07	2.24E+03 \pm 1.24E+01	5.87E+02	2.74E+01 \pm 8.37E+00	1.88E-02	- \pm -
BD+05 2767	13 34 21.50204	+04 40 02 6362	0.70	24.44	8.67E+06	1.07E+07	4.75E+02 \pm 7.54E+00	2.61E+02	2.29E+01 \pm 1.07E+01	9.10E-03	4.97E-13 \pm 2.10E-13
BD-17 3890	13 35 42.2032	-18 15 12.562	0.61	24.24	5.71B+06	6.13E+06	2.40E+02 \pm 2.54E+01	6.79E+01	< 4.08E+01	1.38E-03	- \pm -
HD 118926	13 40 07.13057	-04 11 09.9609	0.70	15.08	6.30E+06	1.07E+07	3.07E+02 \pm 1.67E+01	2.61E+02	< 1.17E+01	9.10E-03	- \pm -
HD 118972	13 41 04.17106	-34 27 50.9872	0.74	15.69	2.69E+07	1.36E+07	> 1.94E+04	5.87E+02	2.11E+02 \pm 2.38E+01	2.52E+00	4.12E-12 \pm 5.30E-13
HD 119332	13 41 13.4047	+56 43 37.821	0.89	23.90	2.85E+07	3.24E+07	-	-	7.48E+01 \pm 2.62E+01	2.52E+00	- \pm -
HD 119291	13 42 26.0345	-01 41 10.577	0.61	24.59	1.45E+07	6.13E+06	1.79E+03 \pm 4.67E+01	6.79E+01	3.66E+01 \pm 1.35E+01	1.38E-03	- \pm -
HD 120476 A	13 49 04.0023	+26 58 47.585	0.74	13.48	2.69E+07	1.36E+07	5.92E+03 \pm 6.78E+00	5.87E+02	1.01E+02 \pm 2.04E+00	1.88E-02	1.59E-12 \pm 2.12E-13

Table 4 continued

Table 4 (continued)

Name ^a	RA	Dec	Mass	Dist.	F_J	σ_J	F_{NUV}	σ_{NUV}	F_{FUV}	σ_{FUV}	f_X		
	2MASS	2MASS	[M_\odot]	[pc]	[μJy]	[μJy]	[μJy]	[μJy]	[μJy]	[μJy]	[erg cm $^{-2}$ s $^{-1}$]		
HD 120780	13 52 35.8602	-50 55 18.124	0.70	16.66	1.59E+07	1.07E+07	> 3.54E+04	2.61E+02	7.90E+01	± 2.16E+01	2.52E+00	4.48E-12 ± 1.42E-12	
BD+13 2721	13 53 27.56205	+12 56 33.4172	0.61	21.92	1.28E+07	6.13E+06	7.18E+02 ± 4.67E+01	6.79E+01	8.42E+01	± 2.64E+01	1.38E-03	— ± —	
HD 122064	13 57 32.05750	+61 29 34.3012	0.79	10.08	1.59E+07	1.82E+07	— ± —	—	2.44E+01	± 4.77E+00	1.22E-01	1.34E-13 ± 4.59E-14	
HD 122120	13 59 19.4031	+22 52 11.104	0.70	23.80	1.59E+07	1.07E+07	2.02E+03 ± 5.06E+01	2.61E+02	< 2.58E+01	9.10E-03	— ± —	—	
HD 124106	14 11 46.17230	-12 36 42.3544	0.86	23.02	2.41E+07	2.71E+07	— ± —	—	1.27E+02 ± 3.05E+01	9.74E-01	5.34E-13	± 1.85E-13	
HD 124642	14 13 55.0781	+30 13 01.872	0.74	17.21	1.74E+07	1.36E+07	4.62E+03 ± 1.61E+01	5.87E+02	7.03E+01	± 1.02E+01	1.88E-02	1.50E-12 ± 3.16E-13	
HD 125455	14 19 34.86361	-05 09 04.2965	0.61	20.46	8.96E+06	6.13E+06	> 1.33E+04	6.79E+01	6.52E+01	± 1.39E+01	9.74E-01	— ± —	
BD+30 2512	14 21 57.2163	+29 37 46.616	0.65	14.52	1.18E+07	7.91E+06	1.23E+03 ± 6.45E+00	1.24E+02	4.83E+01	± 2.25E+00	1.02E-12	± 1.99E-13	
HD 127506	14 30 44.9769	+35 27 13.501	0.74	22.54	1.61E+07	4.27E+03	5.59E+00	5.87E+02	3.78E+01	± 1.67E+00	1.88E-02	8.50E-13 ± 2.98E-13	
HD 127339	14 30 47.71785	-08 38 46.8144	0.61	15.78	8.96E+06	6.13E+06	4.06E+02 ± 1.15E+01	6.79E+01	2.31E+01	± 1.05E+01	1.38E-03	— ± —	
HD 128165	14 33 28.8678	+52 54 31.647	0.79	13.24	1.87E+07	1.82E+07	5.53E+03 ± 1.60E+01	2.23E+03	3.11E+01	± 7.78E+00	4.46E-13	± 8.41E-14	
BD+34 2541	14 34 57.8115	+33 44 48.218	0.65	20.04	9.19E+06	7.91E+06	7.47E+02 ± 1.17E+00	1.24E+02	1.88E+01	± 2.69E+00	5.17E-03	— ± —	
HD 130004	14 45 21.1829	+13 50 46.734	0.89	18.81	1.87E+07	3.24E+07	1.19E+04 ± 1.23E+02	3.07E+04	3.21E+01	± 1.07E+01	2.52E+00	— ± —	
BD+17 2785	14 46 23.2824	+16 29 41.115	0.70	17.76	9.39E+06	1.07E+07	8.55E+02 ± 4.52E+01	2.61E+02	< 2.46E+01	9.10E-03	— ± —	—	
BD+39 2801	14 48 01.4254	+38 27 58.440	0.61	23.99	1.18E+07	6.13E+06	1.01E+03 ± 4.03E+01	6.79E+01	3.05E+01	± 1.10E+01	1.39E-03	1.29E-12 ± 5.26E-13	
HD 130992	14 51 40.46506	-24 18 14.8741	0.74	16.76	1.80E+07	1.36E+07	5.49E+03 ± 5.71E+01	5.87E+02	— ± —	—	—	—	
HD 131582	14 53 41.5706	+23 20 42.630	0.79	23.51	1.70E+07	1.82E+07	6.02E+03 ± 1.48E+02	2.23E+03	7.17E+01	± 2.64E+01	1.22E-01	— ± —	
HD 132142	14 55 11.0436	+53 40 49.246	0.86	23.35	2.75E+07	2.71E+07	— ± —	—	< 2.92E+01	9.74E-01	— ± —	—	
BD+06 2986	15 04 53.5262	+05 38 17.160	0.60	19.02	7.16E+06	5.75E+06	3.88E+02 ± 5.08E+00	5.92E+01	7.77E+00	± 1.35E+00	1.38E-03	— ± —	
BD-04 3873	15 22 04.10086	-04 46 38.8234	0.74	19.18	9.40E+06	1.36E+07	7.70E+02 ± 4.09E+01	5.87E+02	3.32E+01	± 1.32E+01	1.88E-02	— ± —	
HD 137339	15 25 58.50235	-26 42 20.8264	0.74	22.16	1.41E+07	1.36E+07	2.97E+03 ± 3.74E+01	5.87E+02	< 5.39E+01	1.88E-02	— ± —	—	
HD 137778	15 28 12.21068	-09 21 28.2944	0.86	20.67	5.01E+07	2.71E+07	> 2.75E+04	1.34E+04	2.40E+02	± 2.97E+01	9.74E-01	4.52E-12 ± 6.20E-13	
HD 139477	15 35 20.04338	+60 05 13.171	0.79	19.55	1.59E+07	1.82E+07	4.61E+03 ± 5.32E+01	2.23E+03	9.67E+01	± 1.28E+01	1.22E-01	7.46E-12 ± 4.47E-13	
HD 139323	15 35 56.5662	+39 49 52.027	0.79	22.47	3.17E+07	1.82E+07	1.72E+04 ± 1.29E+02	2.23E+03	5.74E+01	± 1.15E+01	1.22E-01	2.00E-12 ± 4.81E-13	
HD 139341	15 36 02.22306	+39 48 08.9141	0.86	22.32	5.01E+07	2.71E+07	— ± —	—	1.07E+02	± 1.40E+01	9.74E-01	— ± —	
HD 142709	15 57 40.74436	-42 27.2394	0.74	14.73	1.36E+07	1.36E+07	1.78E+03 ± 4.17E+01	5.87E+02	— ± —	—	—	—	
HD 144628	16 09 42.7946	-56 26 42.542	0.65	14.83	1.16E+07	7.91E+06	> 4.40E+04	1.24E+02	6.55E+01	± 4.26E+00	2.52E+00	— ± —	
14 Her	16 10 23.145	+43 49 03.522	0.65	17.94	1.17E+07	7.91E+06	> 3.16E+04	1.24E+02	5.87E+02	± 1.71E+00	9.10E-03	— ± —	
BD+41 2695	16 20 52.7395	+40 57 41.221	0.70	15.79	9.78E+06	1.07E+07	6.49E+02 ± 5.84E+00	2.61E+02	6.79E+01	± 1.51E+01	1.38E-03	— ± —	
HD 147555	16 24 27.28476	-43 39 23.7163	0.65	29.45	1.16E+07	7.91E+06	9.86E+02 ± 6.07E+01	1.24E+02	— ± —	—	—	—	
HD 148467	16 27 56.5072	+07 18 19.598	0.65	17.53	1.17E+07	1.82E+07	1.05E+03 ± 2.43E+01	5.87E+02	— ± —	—	—	—	
HD 151541	16 42 38.5765	+68 06 17.792	0.61	24.35	9.47E+06	6.13E+06	> 3.00E+04	6.79E+01	5.48E+01	± 1.09E+01	9.74E-01	— ± —	
BD+39 3048	16 49 24.6974	+39 13 34.476	0.74	18.35	1.36E+07	8.06E+02 ± 1.01E+01	5.87E+02	2.37E+01	3.45E+00	1.88E-02	— ± —	—	
Ross 644	16 54 12.03227	+11 54 52.857	0.61	20.08	4.51E+06	6.13E+06	1.21E+02 ± 1.51E+01	6.79E+01	< 1.79E+01	1.38E-03	— ± —	—	
HD 154712B	17 03 19.78133	+59 35 15.9688	0.74	24.96	8.48E+06	1.36E+07	< 5.33E+00	5.87E+02	2.73E+01 ± 3.36E+00	1.88E-02	6.39E-13 ± 1.41E-13	—	
BD+54 1862	17 10 12.3543	+54 29 24.506	0.60	21.24	1.12E+07	5.75E+06	1.26E+03 ± 5.13E+01	5.92E+01	1.40E+01	± 4.76E+00	5.17E-03	— ± —	
HD 155712	17 12 37.62262	+18 21 04.3072	0.79	20.84	2.22E+07	1.82E+07	> 3.07E+04	6.79E+00	2.66E+01	± 2.24E+00	1.22E-01	— ± —	
HD 156668	17 17 40 49.053	+29 13 38.0243	0.79	21.35	8.73E+06	3.28E+03	8.06E+02 ± 3.40E+01	2.23E+03	< 5.12E+01	1.22E-01	— ± —	—	
HD 156985	17 17 50 42.36	+52 26 49.609	0.83	18.53	1.94E+07	2.27E+07	7.04E+02 ± 6.63E+01	5.21E+03	5.09E+01	± 1.58E+01	2.48E-01	— ± —	
BPM 78873	17 18 21.72350	-01 46 53.2502	0.61	22.51	7.68E+06	6.13E+06	3.58E+02 ± 1.89E+01	6.79E+01	1.08E+02	± 3.31E+01	1.38E-03	7.31E-13 ± 2.07E-13	
HD 158633	17 25 00.0975	+67 18 24.148	0.79	12.79	1.93E+07	1.82E+07	> 6.09E+04	2.23E+03	6.89E+01	± 9.33E+00	2.52E+00	— ± —	
GJ 673	17 25 45.2323	+02 06 41.122	0.61	22.19	1.01E+07	6.13E+06	6.82E+02 ± 7.17E+00	6.79E+01	2.74E+01	± 4.04E+00	1.38E-03	4.11E-13 ± 7.45E-14	
HD 162283	17 50 34.0331	-06 03 01.037	0.61	24.32	1.93E+07	8.73E+06	6.13E+06	4.45E+02 ± 4.07E+01	6.79E+01	< 5.12E+01	1.22E-01	— ± —	—
BD+21 3245	17 53 29.9358	+21 19 31.053	0.79	24.52	1.82E+07	1.93E+07	1.16E+04 ± 8.23E+01	2.23E+03	2.33E+02 ± 2.31E+01	1.22E-01	1.90E-12 ± 4.11E-13	—	
G 204-45	18 07 44.4478	+39 04 26.915	0.70	22.64	1.59E+07	1.07E+07	1.37E+03 ± 3.32E+01	2.61E+02	< 2.71E+01	9.10E-03	3.44E-13 ± 1.22E-13	—	
Wolf 1409	18 07 51.3998	+52 47 54.658	0.70	28.36	1.87E+06	1.07E+07	3.08E+01 ± 1.14E+01	2.61E+02	< 2.76E+01	9.10E-03	— ± —	—	
HD 166620	18 09 37.41626	+38 27 27.9960	0.61	11.10	9.21E+06	6.13E+06	1.40E+02 ± 2.24E+01	6.79E+01	2.55E+01 ± 5.08E+00	2.45E-01	— ± —	—	
G 205-20	18 25 31.92818	+38 21 12.6762	0.65	23.60	4.31E+06	7.91E+06	1.40E+02 ± 2.24E+01	1.24E+02	< 2.92E+01	5.17E-03	— ± —	—	

Table 4 continued

Table 4 (continued)

Name ^a	RA	Dec	Mass	Dist.	F_J	σ_J	F_{NUV}	σ_{NUV}	F_{FUV}	σ_{FUV}	f_X
	2MASS	2MASS	[M_\odot]	[pc]	[μJy]	[μJy]	[μJy]	[μJy]	[μJy]	[μJy]	[$\text{erg cm}^{-2} \text{s}^{-1}$]
HD 171314	18 33 17.7601	+22 18 51.312	0.74	23.39	1.64E+07	1.36E+07	2.26E+03 \pm 2.96E+01	5.87E+02	< 2.10E+01	1.88E-02	— ± —
HD 225950	18 48 51.8715	+17 26 20.208	0.61	16.68	9.21E+06	6.13E+06	5.44E+02 \pm 1.16E+01	6.79E+01	2.60E+01 \pm 9.84E+00	1.38E-03	— ± —
HD 178445	19 10 52.26921	-47 09 31.0178	0.61	20.78	1.26E+07	6.13E+06	7.78E+02 \pm 3.09E+01	6.79E+01	< 1.75E+01	1.38E-03	— ± —
HD 183870	19 32 06.7042	-11 16 29.790	0.61	17.69	4.23E+06	6.13E+06	> 5.60E+04	6.79E+01	1.24E+02 \pm 1.33E+01	2.44E-01	— ± —
sig Dra	19 32 21.5899	+69 39 40.236	0.89	5.77	2.28E+07	3.24E+07	— ± —	4.66E+01 \pm 3.15E+00	2.52E+00	4.07E-13 \pm 2.05E-14	— ± —
HD 332518	19 45 35.6050	+30 00 36.784	0.70	20.93	1.19E+07	1.07E+07	1.15E+03 \pm 4.92E+01	2.61E+02	— ± —	—	— ± —
LHS 3517	20 04 10.90	-45 39 09.9	0.61	36.88	4.23E+06	6.13E+06	1.10E+02 \pm 2.50E+01	6.79E+01	< 4.37E+01	1.38E-03	— ± —
HD 1932061	20 10 52.41566	+77 14 20.3031	0.61	16.82	1.23E+07	6.13E+06	8.38E+02 \pm 5.90E+00	6.79E+01	3.73E+01 \pm 6.03E+00	1.24E-13 \pm 3.58E-14	— ± —
HD 192961	20 19 36.93546	-46 25 41.2315	0.65	18.47	1.34E+07	7.91E+06	1.32E+03 \pm 3.19E+01	6.79E+01	2.01E+01 \pm 6.44E+00	5.17E-03	— ± —
CD-52 9466	20 21 10.91759	-51 47 27.8274	0.61	28.66	1.54E+07	6.13E+06	9.07E+02 \pm 2.97E+01	6.79E+01	8.17E+01 \pm 2.45E+01	1.38E-03	— ± —
HD 196877	20 42 18.78232	-52 41 57.3427	0.61	12.33	7.49E+06	6.13E+06	3.69E+02 \pm 1.20E+01	6.79E+01	< 7.32E+00	1.38E-03	— ± —
HD 352860	20 44 21.94494	+19 44 58.8712	0.65	20.60	7.70E+06	7.91E+06	5.29E+02 \pm 2.54E+01	1.24E+02	2.51E+01 \pm 9.30E+00	5.17E-03	— ± —
HD 198550	20 50 10.5456	+29 23 02.915	0.70	20.23	1.05E+07	6.13E+06	4.83E+03 \pm 6.39E+01	2.61E+02	— ± —	—	— ± —
BD+52 2815	20 50 33.0757	+52 53 54.545	0.61	22.74	1.05E+07	6.13E+06	5.44E+02 \pm 4.16E+01	6.79E+01	— ± —	—	— ± —
HD 200779	21 05 19.7460	+07 04 09.471	0.65	15.05	1.38E+06	7.91E+06	1.31E+03 \pm 2.49E+01	1.24E+02	3.73E+01 \pm 5.27E+00	5.17E-03	— ± —
HD 202575	21 16 32.4670	+09 23 37.776	0.79	16.16	1.56E+07	1.82E+07	5.29E+03 \pm 1.82E+01	2.23E+03	9.13E+01 \pm 6.92E+00	1.22E+01	9.17E-13 \pm 2.83E-13
GJ 825	21 17 15.26879	-38 52 02.4958	0.61	3.97	6.05E+06	6.13E+06	3.05E+02 \pm 2.59E+00	6.79E+01	9.85E+00 \pm 7.86E-01	1.38E-03	1.04E-13 \pm 1.41E-14
HD 203850	21 26 58.45314	-56 07 30.9477	0.79	23.06	1.41E+07	1.82E+07	7.86E+03 \pm 7.28E+01	2.23E+03	— ± —	—	— ± —
HD 205390	21 36 41 24416	-50 50 43.3591	0.86	14.81	2.17E+07	2.71E+07	— ± —	—	9.71E+01 \pm 9.80E+00	9.74E-01	9.07E-13 \pm 1.85E-13
HD 207144	21 48 00.04545	-40 15 21.8898	0.79	24.50	1.77E+07	1.82E+07	6.59E+03 \pm 6.86E+01	2.23E+03	9.13E+01 \pm 6.92E+00	1.22E+01	9.17E-13 \pm 2.83E-13
HD 207491	21 49 12.228	+05 43 22.97	0.79	22.56	1.57E+07	1.82E+07	4.50E+03 \pm 6.62E+01	2.23E+03	4.35E+01 \pm 1.11E+01	1.22E+01	— ± —
HD 208038	21 53 05.3533	+20 55 49.871	0.79	23.30	2.11E+07	1.82E+07	4.16E+04 \pm 4.69E+01	2.23E+03	1.54E+02 \pm 2.43E+01	1.22E+01	5.47E-12 \pm 1.08E-12
LP 758-73	21 53 07.5400	-12 49 10.845	0.61	24.12	4.92E+06	6.13E+06	2.10E+02 \pm 6.79E+00	6.79E+01	< 1.76E+01	1.38E-03	— ± —
CD-61 6651	21 59 32.09420	-60 35 58.7116	0.65	23.73	1.16E+07	7.91E+06	8.61E+02 \pm 2.55E+01	1.24E+02	< 1.11E+01	5.17E-03	— ± —
G 127-28	22 24 45.53616	+22 33 04.0636	0.61	20.92	1.76E+07	1.76E+07	2.29E+03 \pm 5.03E+01	6.79E+01	4.02E+01 \pm 1.19E+01	4.45E-13 \pm 1.40E-13	— ± —
HD 213042	22 29 15.25549	-30 01 06.2712	0.74	15.69	1.93E+07	1.36E+07	3.74E+03 \pm 4.38E+01	5.87E+02	2.78E+01 \pm 5.48E+00	1.88E-02	— ± —
HD 214731	22 40 58.70043	-46 12 07.1842	0.74	23.30	1.25E+07	1.36E+07	— ± —	—	< 1.44E+01	1.88E-02	— ± —
HD 215152	22 43 21.3028	-06 24 02.953	0.79	21.61	2.14E+07	1.82E+07	— ± —	—	1.92E+01 \pm 9.49E+00	1.22E+01	— ± —
HD 216520	22 47 31.8769	+83 41 49.302	0.65	19.56	1.29E+07	7.91E+06	> 1.26E+04	1.24E+02	3.97E+01 \pm 1.67E+01	2.52E+00	— ± —
HD 216259	22 51 26.3584	+13 58 11.941	0.79	22.54	1.83E+07	1.82E+07	— ± —	—	1.91E+01 \pm 3.19E+00	1.22E+01	— ± —
GJ 879	22 56 24.05327	-31 33 56.0351	0.74	7.61	1.42E+07	1.36E+07	— ± —	—	9.91E+01 \pm 4.82E+00	1.38E-02	1.88E-02
HD 218511	23 09 40.95125	-67 43 58.1682	0.65	14.84	1.29E+07	7.91E+06	1.73E+03 \pm 3.65E+01	1.24E+02	— ± —	—	— ± —
HD 219538	23 16 18.1577	+30 40 12.743	0.83	24.91	2.56E+07	2.27E+07	1.98E+04 \pm 9.67E+01	5.21E+03	5.63E+01 \pm 1.04E+01	2.45E-01	— ± —
HD 220339	23 23 04.8953	-10 45 51.2777	0.83	19.18	1.94E+07	2.27E+07	— ± —	—	3.49E+01 \pm 2.26E+00	2.45E-01	— ± —
HD 221503	23 32 49.3982	-16 50 44.321	0.65	14.56	1.08E+07	7.91E+06	1.28E+03 \pm 1.76E+01	1.24E+02	7.29E+01 \pm 6.00E+00	5.17E-03	— ± —
BD+00 5017	23 35 00.2759	+01 36 19.455	0.61	20.82	1.22E+07	6.13E+06	1.52E+03 \pm 9.57E+00	6.79E+01	1.73E+02 \pm 4.62E+00	1.38E-03	1.12E-11 \pm 1.03E-12
CD-49 14193	23 36 18.27486	-48 35 17.0609	0.61	25.04	1.05E+07	7.91E+06	6.69E+02 \pm 2.57E+01	6.79E+01	5.17E+01 \pm 1.41E+01	4.01E-13 \pm 9.14E-14	— ± —
BD-03 5691	23 42 10.62469	-02 34 36.6880	0.61	24.29	7.98E+06	6.13E+06	5.61E+03 \pm 1.64E+01	6.79E+01	8.04E+01 \pm 3.36E+00	1.38E-03	— ± —
G 130-9	23 45 49.5010	+36 15 18.4779	0.74	19.82	7.39E+06	1.36E+07	4.46E+03 \pm 1.24E+01	5.87E+02	< 1.00E+01	1.88E-02	— ± —
BD+29 5007	23 50 29.28618	+30 21 11.731	0.70	23.65	1.30E+07	1.07E+07	1.92E+03 \pm 2.22E+01	2.61E-02	7.83E+01 \pm 1.27E+01	9.10E-03	— ± —
BD+28 4660	23 53 08.5916	+29 01 05.034	0.65	19.91	8.57E+06	7.91E+06	6.82E+02 \pm 3.85E+01	1.24E+02	< 1.00E+01	5.17E-03	— ± —
BD+45 4378	23 58 43.50974	+46 43 44.9540	0.61	17.12	1.01E+07	6.13E+06	3.68E+02 \pm 1.75E+01	6.79E+01	— ± —	—	— ± —

^a Names starting with J are 2MASS objects.